

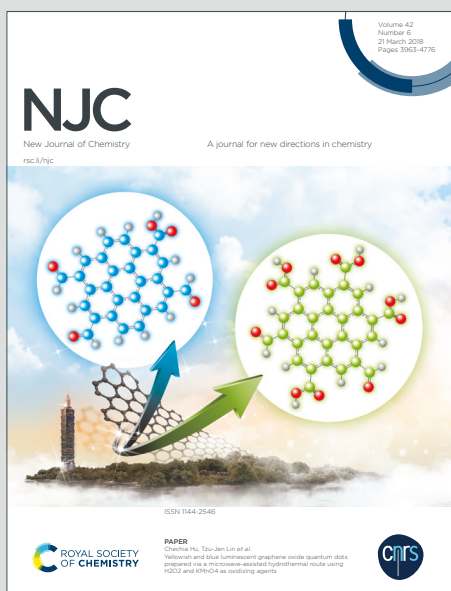
NJC

New Journal of Chemistry

Accepted Manuscript

A journal for new directions in chemistry

This article can be cited before page numbers have been issued, to do this please use: R. Tomer and P. Biswas, *New J. Chem.*, 2020, DOI: 10.1039/D0NJ04151C.



This is an Accepted Manuscript, which has been through the Royal Society of Chemistry peer review process and has been accepted for publication.

Accepted Manuscripts are published online shortly after acceptance, before technical editing, formatting and proof reading. Using this free service, authors can make their results available to the community, in citable form, before we publish the edited article. We will replace this Accepted Manuscript with the edited and formatted Advance Article as soon as it is available.

You can find more information about Accepted Manuscripts in the [Information for Authors](#).

Please note that technical editing may introduce minor changes to the text and/or graphics, which may alter content. The journal's standard [Terms & Conditions](#) and the [Ethical guidelines](#) still apply. In no event shall the Royal Society of Chemistry be held responsible for any errors or omissions in this Accepted Manuscript or any consequences arising from the use of any information it contains.

1
2
3 **Dehydration of glucose/fructose to 5-Hydroxymethylfurfural (5-HMF) over an easily** View Article Online
4 DOI: 10.1039/C0NJ04151C
5 **recyclable sulfated titania (SO₄²⁻/TiO₂) catalyst**
6
7
8
9
10
11
12
13
14
15
16
17
18
19
20
21
22
23
24
25
26
27
28
29
30
31
32
33
34
35
36
37
38
39
40
41
42
43
44
45
46
47
48
49
50
51
52
53
54
55
56
57
58
59
60

Richa Tomer and Prakash Biswas*

Department of Chemical Engineering, Indian Institute of Technology Roorkee,

Roorkee 247667, Uttarakhand, India.

*Corresponding Author: Tel.: (+91)-1332-28-5820; Fax: (+1)-1332-27-6535

E-mail: prakash.biswas@ch.iitr.ac.in; prakashbiswas@gmail.com

AbstractView Article Online
DOI: 10.1039/D0NJ04151C

A new $\text{SO}_4^{2-}/\text{TiO}_2$ catalyst was developed by sol-gel hydrolysis followed by the wetness impregnation method. The Lewis (L) and Brønsted (B) site's proportion in the catalyst was tuned with the variation of sulfate ion concentration in the catalyst. The dehydration of glucose/fructose to 5-hydroxymethylfurfural (5-HMF) was evaluated in a batch reactor in the presence of organic and/or aqueous medium at different temperatures (100-180 °C) and reaction time (1- 8 h). The 0.5 M $\text{SO}_4^{2-}/\text{TiO}_2$ catalyst was found to be very efficient, which demonstrated 100% conversion of glucose/fructose with a maximum 5-HMF yield of ~37%, and ~75%, respectively, at 150 °C and after 6 h of reaction. Results depicted that the proportion of Lewis and/or Brønsted acidic strength of catalyst played a crucial role in the yield of 5-HMF. The presence of water in the reaction medium demonstrates a negative effect on the 5-HMF yield and glucose/fructose conversion. Further, a new catalyst regeneration strategy was developed and it has been established that 0.5 M $\text{SO}_4^{2-}/\text{TiO}_2$ catalyst can be regenerated completely and can be reused several times with constant activity and 5-HMF yield. Kinetic study of glucose dehydration reaction over 0.5 M $\text{SO}_4^{2-}/\text{TiO}_2$ catalyst suggested a second-order kinetic model with an activation energy of 195.4 kJ mol⁻¹.

Keywords: Glucose dehydration, 5-HMF, $\text{SO}_4^{2-}/\text{TiO}_2$ catalysts, DMSO, catalyst regeneration.

1. Introduction

View Article Online
DOI: 10.1039/D0NJ04151C

In very recent, the production of valuable chemicals, fuels, and fuel additives from renewable sources such as biomass has received significant attention because of the depletion of fossil fuel resources and most importantly the environmental consequences.¹ The cellulose fraction (~35-50%) of biomass is the potential source of glucose, which can be a promising candidate for the production of various high-priced finished products and intermediates such as 5-hydroxymethylfurfural (5-HMF), formic acid (FA), levulinic acid (LA), lactic acid, acetic acid, gluconic acid, etc.² Among all these chemicals, 5-HMF has been identified as the most valuable chemical intermediate and it also has been regarded as a top ten building block chemical globally.³ 5-HMF can be a feedstock of fine chemicals and biofuel additives such as levulinic acid, 2,5-diformylfuran (DFF), dihydroxymethylfuran (DMF), and 2,5-furandicarboxylic acid (FDCA), etc.^{2,4} 5-HMF can also be reduced catalytically to a high calorific (31.5 MJ L⁻¹) biofuel 2, 5-dimethylfuran (DMF).⁵ At present, the production cost of 5-HMF and the byproducts formation limits its availability. Therefore, a process for the production of 5-HMF from renewable carbohydrates with low energy input is highly desirable.

Various recent studies reported very high yield (98.6%) of 5-HMF from fructose,⁶ although fructose is not recommended as a model feedstock due to its inflated price and less availability. As a result, low cost and abundantly available glucose is a more preferred feedstock for the production of 5-HMF.^{1,7} The formation of 5-HMF from glucose is a two-step process i.e. isomerization of glucose to fructose followed by the dehydration fructose to 5-HMF with the elimination of three water molecules in presence of a catalyst. It has been shown that the presence of both the Brønsted and Lewis acid sites in the catalyst is essential for the formation of 5-HMF via glucose isomerization and dehydration steps, respectively.⁸

Various previous reports presented heterogeneous glucose dehydration in the presence of different reaction media such as aqueous,⁹ organic,^{10,11} biphasic,¹² ionic liquids,¹³ and hot

1
2
3 compressed water.¹⁴ Aqueous medium manifested a detrimental effect on the yield of 5-HMF¹⁵ and the organic solvents such as dimethylsulfoxide (DMSO), methyl isobutyl ketone (MIBK),
4
5
6 tetrahydrofuran (THF), dimethylformamide (DMF) are generally reported as good for glucose
7
8 dehydration. Among the organic solvents, DMSO is reported as one of the most suitable ones
9
10 because of its better dehydration ability,¹⁶ favorable solvation property,¹¹ and suppression of
11
12 side reactions ability.^{17,18} Moreover, many studies reported an efficient 5-HMF yield in ionic
13
14 liquid as a solvent.¹⁹ The elevated price of ionic liquids and its ineffective product separation
15
16 ability make it less attractive.²⁰ As a promising alternative, recently, many studies focused on
17
18 the biphasic reaction medium.²¹ However, high extraction efficiency and high solvent
19
20 recyclability is the key issue in the biphasic medium.²²

21
22
23 Solid acid catalysts with a tunable Lewis and Brønsted acid sites,²³ zeolites,^{24,25}
24
25 heteropolyacids,²⁶ metal oxides,²⁷ sulfated and phosphate metal oxides,^{13,18,28} transition metals⁹
26
27 have been evaluated for the synthesis of 5-HMF via glucose dehydration. Yan et al.¹⁸ reported
28
29 a 5-HMF yield of 47.5% with 97.2% conversion of glucose in the DMSO solvent in presence
30
31 of $\text{SO}_4^{2-}/\text{ZrO}_2\text{-Al}_2\text{O}_3$ catalyst. The basic strength of the catalyst increased with increasing the
32
33 alumina content, which enhanced glucose isomerization to fructose. However, the stability of
34
35 this catalyst was an issue. Hydrotalcite in combination with Amberlyst-15 was tested for
36
37 glucose dehydration in presence of various organic solvents including water, DMF, acetonitrile
38
39 (MeCN), DMSO, and dimethylacetamide (DMA).²⁹ The basic hydrotalcite is served for
40
41 isomerization and acidic Amberlyst-15 served for dehydration reaction, respectively. The
42
43 presence of both the catalysts was essential for the selective conversion of glucose to 5-HMF.
44
45 A maximum 5-HMF selectivity to 61% was obtained in the DMSO medium, and the selectivity
46
47 was nil in the aqueous medium because of the deactivation of Amberlyst-15 in water. Qu et
48
49 al.³⁰ used $[\text{CO}_2\text{HMIM}]\text{BF}_4$ ionic liquid as a catalyst in the DMSO medium and obtained a very
50
51 good yield (67.4%) of 5-HMF at 180 °C in N_2 atmosphere, due to its stabilizing effect of the
52
53
54
55
56
57
58
59
60

1
2
3 ionic liquid. However, the extraction of 5-HMF from the reaction mixture was difficult. Otomo
4 et al.²⁴ disclosed a 55% yield of 5-HMF with β -zeolite at 180 °C in a water-DMSO-THF
5 medium after 3 h. It has reported that water and DMSO favored the dissolution of glucose
6 molecules, DMSO suppressed the side reactions of fructose and THF used for the extraction of
7 5-HMF from the water medium during the reaction. Liu et al.³¹ varied the Al/B molar ratio in
8 an Al_n-B_{10-n} catalyst and obtained a maximum 41.4% yield of 5-HMF in the DMSO medium
9 at the Al: B molar ratio of 5:5. It has been shown that the surface area and acidity increased
10 with increasing the boron amount in the catalyst and it was highest at the Al: B ratio of 5:5.
11 The surface area and acidity of the catalyst affected the 5-HMF selectivity and glucose
12 conversion significantly. However, catalyst leaching was reported as a major problem. Lu et
13 al.¹⁷ reported that partially hydroxylated AlF₃ was extremely useful for the production of 5-
14 HMF due to the presence of both the Brønsted and Lewis acid centers and reported a 57.3%
15 yield of 5-HMF with 95.5% conversion of glucose in the DMSO medium at 140 °C and after
16 10 h of reaction. Shahangi et al.¹¹ synthesized fibrous nanosphere Al-KCC-1 silica catalyst and
17 obtained a 39% yield of 5-HMF with 97.8% conversion of glucose in the DMSO solvent at
18 170 °C. Textural properties and the acidity of the catalyst are reported as the primary factors
19 for higher activity and good selectivity to 5-HMF. DMSO was reported as a better solvent due
20 to its more polarity. He et al.¹⁰ reported 34% selectivity to 5-HMF at the complete conversion
21 of glucose in DMSO. Highly porous SiO₂-ZrO₂ based amide hollow fiber demonstrated
22 aminosilane grafting increased the porosity of the catalyst. The presence of both the Lewis and
23 Brønsted acidic sites on the catalyst was reported as the most influencing factor for high 5-
24 HMF selectivity and glucose conversion. Feng et al.²⁸ showed a 25.8% yield of 5-HMF over
25 sulfated zirconia modified with H⁺ zeolites in DMSO and the yield increased to 61.6% when
26 NaCl-H₂O-DMSO was used as a solvent. The inclusion of water as a solvent increased glucose
27 dissolution, which enhanced 5-HMF yield because of the salting-out effect of saturated NaCl
28
29
30
31
32
33
34
35
36
37
38
39
40
41
42
43
44
45
46
47
48
49
50
51
52
53
54
55
56
57
58
59
60

1
2
3 solution. Halide ion acted as a base and nucleophile to facilitate the dehydration of fructose to
4
5 5-HMF.³² View Article Online
DOI: 10.1039/D0NJ04151C

6
7
8 The primary objective of this study was to develop an acceptable catalyst and process
9
10 for glucose and fructose dehydration to 5-HMF in the DMSO medium. In this study, anatase
11
12 TiO₂ was synthesized by the sol-gel hydrolysis method and this TiO₂ was functionalized with
13
14 the sulfate group by wetness impregnation technique. The sulfated titania catalyst was tested
15
16 for dehydration of glucose to 5-HMF in the DMSO solvent and the results were compared
17
18 with fructose dehydration. The effect of various reaction parameters including temperature,
19
20 time, catalyst amount, water to DMSO ratio was evaluated. Results demonstrated that among
21
22 all other 0.5 M SO₄²⁻/TiO₂ catalyst was very effective for selective conversion of glucose and
23
24 fructose to 5-HMF. The catalyst reusability and stability were also explored, and the results
25
26 were analyzed in light of the fresh and used catalysts characterization data, respectively. A
27
28 new catalyst regeneration strategy is developed and the results suggested that the sulfated
29
30 catalyst can be regenerated completely after each cycle and can be used in several cycles with
31
32 constant activity and 5-HMF yield.

33 34 35 36 37 38 39 40 41 42 43 44 45 46 47 48 49 50 51 52 53 54 55 56 57 58 59 60

2. Experimental

2.1 Catalyst synthesis

Anatase TiO₂ and SO₄²⁻/TiO₂ were synthesized by the sol-gel hydrolysis technique^{33,34}
with some modification. In a typical TiO₂ synthesis, titanium isopropoxide, [Ti(OPr)₄] (98%
Avra Synthesis, India), and isopropanol (99%, Thomas Baker, India) at the volume ratio of 1:2
were mixed in a beaker and the excess amounts of water (~100 mL, hydrolysis ratio of 31.7)
was added dropwise to the mixture under constant stirring for 2 h. The obtained white
suspension was kept at room temperature overnight for aging. The resulting solution was
filtered and the solids in the filtrate were washed thoroughly by deionized water to remove the

alkoxide accompanied by overnight drying at 80 °C in a hot air oven. The light, fluffy and white powder obtained after drying was calcined at three different temperatures i.e. at 400, 500, and 600 °C, respectively, for 3 h in presence of air to obtain the anatase TiO₂. The anatase form of TiO₂ was more intense for the TiO₂ calcined at 500 °C.

To induce the Brønsted acid sites to the anatase TiO₂ powder, sulfation was performed by the wetness impregnation method. In this process, the required amounts of TiO₂ powder was added to 1 M H₂SO₄ [98%, Thomas Baker, India] solution (~50 mL) and stirred for 2 h at room temperature. The resulting slurry was kept in a hot-air oven maintained at 80 °C for overnight to evaporate excess water. Further, the dried powder obtained was grounded in a mortar and pestle followed by calcination for 3 h at 500 °C in air. The resulting solid dry catalyst powder was labeled as 1 M SO₄²⁻/TiO₂. Similarly, the catalyst with different sulfate concentrations i.e. 0.75 M SO₄²⁻/TiO₂, 0.50 M SO₄²⁻/TiO₂, and 0.25 M SO₄²⁻/TiO₂ were prepared only by varying the H₂SO₄ concentration in the impregnation step.

2.2 Catalyst characterization

The characteristics of the catalysts were determined by several characterization techniques. The textural properties i.e. surface area and pore-size distribution of the catalysts were analyzed in an ASAP-2060 instrument (Micromeritics, USA). The N₂ adsorption-desorption isotherms were obtained at the liquid nitrogen temperature of -196 °C. The surface area was determined by the Brunauer-Emmett-Teller (BET) procedure and the pore size was measured by following the Barret-Joyner-Halenda (BJH) technique. Before each analysis, the degassing of the catalyst powder was performed for 2 h at 200 °C under vacuum.

The X-ray diffraction (XRD) study of the catalyst was performed in a Bruker diffractometer (D8-Advance, Germany) with Cu-K α radiation ($\lambda = 1.5406 \text{ \AA}$) generated at 40

1
2
3 kV and 40 mA, respectively. The data were collected at the 2θ range of 5 to 90° with a step of View Article Online
DOI: 10.1039/C9NJ04151C
4
5 0.02° and a scanning rate of $10^\circ \text{ min}^{-1}$.
6
7

8 Thermogravimetric analysis (TGA) was performed in an EXSTAR TG/DTG 6300
9 instrument (Japan) under the nitrogen flow of 200 mL min^{-1} . The powder catalyst was heated
10 from room temperature to 900°C at the rate of $10^\circ \text{C min}^{-1}$.
11
12

13 The surface morphology was determined by Field Emission Scanning electron
14 microscope (FE-SEM) by Carl Zeiss (Carl Zeiss Ultra Plus Model, Germany) equipped with
15 energy dispersive X-ray spectra (EDX). Powder catalyst was dispersed on a sample holder
16 followed by gold coating by using a sputter coater (Edwards S150). Further, the SEM images
17 were captured at an acceleration voltage of 20 kV under a vacuum. The morphology of the
18 catalysts was also recorded in a TEM (Tecnai G² 20 S-Twin, FEI Model, USA). The TEM
19 instrument was coupled with an energy dispersive spectroscopy (EDX) electron mapping.
20 Energy-dispersive X-ray spectroscopy (EDX) was used to quantify the surface elemental
21 composition. Prior to TEM analysis, the catalyst powder was disseminated in alcohol with
22 ultra-sonication for 15 minutes and put on the copper grid.
23
24
25
26
27
28
29
30
31
32
33
34
35
36
37
38
39
40
41
42
43
44
45
46
47
48
49
50
51
52
53
54
55
56
57
58
59
60

1 The total acidic strength of the catalysts was measured by NH_3 temperature-
2 programmed desorption (NH_3 -TPD) analysis in a Micromeritics chemisorb-2750 instrument
3 (Micromeritics instrument corporation, USA) equipped with a thermal conductivity detector.
4 In a typical NH_3 -TPD analysis, approximately 300-400 mg of sample was loaded in a U-tube
5 quartz reactor and degassed the sample at 200°C for 2 h under the flow of helium (20 mL
6 min^{-1}), accompanied by cooling to atmospheric temperature. Further, the degassed sample was
7 saturated with NH_3 by purging the mixture gas (10% NH_3 -He) over the catalyst sample for 45
8 min at 20 mL min^{-1} . After NH_3 saturation, the surplus ammonia was removed by flushing the
9 tube with pure helium (20 mL min^{-1}) for 1 h. Further, the catalyst was heated up to 1000°C at
10
11
12
13
14
15
16
17
18
19
20
21
22
23
24
25
26
27
28
29
30
31
32
33
34
35
36
37
38
39
40
41
42
43
44
45
46
47
48
49
50
51
52
53
54
55
56
57
58
59
60

1
2
3 a rate of 10 °C min⁻¹. The amounts of desorbed NH₃ was monitored by using a thermal
4 conductivity detector connected with chemisoft-tpx software. View Article Online
DOI: 10.1039/C9NJ04151C

5
6
7
8 To analyze the chemical state of titania and sulfur on the solid surface, X-ray
9 photoelectron spectroscopy (XPS) was performed in PHI 5000 Versa Probe-III scanning XPS
10 microscopy (USA) with Al-K- α line excitation source. The recorded spectra were calibrated
11 by the characteristic binding energy of C 1s at 284.0 eV.

12
13
14
15
16
17
18
19
20
21
22
23
24
25
26
27
28
29
30
31
32
33
34
35
36
37
38
39
40
41
42
43
44
45
46
47
48
49
50
51
52
53
54
55
56
57
58
59
60
Fourier transform infrared spectroscopy (FT-IR) was carried out in Thermo Nicolet
6700 FT-IR spectrometer (USA) to determine the functional group attached to TiO₂ and sulfate
functionalized TiO₂. Pellets of the dried sample were made with KBr and scanned in the ranges
of 400-4000 cm⁻¹ at 25°C.

Pyridine FTIR was recorded on a Bruker Tensor II spectrophotometer (Bruker,
Germany). In a typical procedure, 50 mg of catalyst sample was dried at 120°C for 1 h and
cooled to 25°C under vacuum. Then the vacuum dried sample was saturated in 0.1 mL of
pyridine in a vial and kept for 1 h to complete the pyridine adsorption process, followed by
evaporation of excess pyridine at 120°C for 1 h in an oven. Typically, 95 mg of KBr was mixed
with 5 mg of pyridine treated sample and pressed into a self-supporting wafer of 13 mm
diameter, and the weight of the pallet was measured. Further, the wafer was mounted in the IR
cell and scanned in the ranges of 500-4000 cm⁻¹ with 32 scans at a resolution of 4 cm⁻¹. The
concentration of Lewis and Brønsted acid sites on the catalyst was calculated based on the
method described elsewhere.^{7,35}

2.3 Catalytic test

The performance of different catalysts (TiO₂, 0.25 M SO₄²⁻/TiO₂, 0.5 M SO₄²⁻/TiO₂,
0.75 M SO₄²⁻/TiO₂, 1 M SO₄²⁻/TiO₂) for the dehydration of glucose/fructose to 5-
hydroxymethylfurfural (5-HMF) was evaluated in a 100 mL round bottom glass reactor

1
2
3 equipped with a condenser and a magnetic stirrer (Digital Hot Plate, Tarsons, India) connected View Article Online
DOI: 10.1039/C9NJ04151C
4
5 with a temperature controller and thermocouples. Thermocouples were used to measure the
6
7 temperature of the oil bath as well as the reaction mixture. In the vertical glass condenser (400
8
9 mm), cold water (~25°C) was continuously circulated at a volumetric flow rate of 200±5 mL
10
11 min⁻¹ through its spiral circulating path during the reaction. The predetermined amount of
12
13 reactant (10 wt.% of solvent) and the catalyst was added to the reactor placed in an oil bath.
14
15 Glass reactor was placed in the oil bath after achieving the desired reaction temperature. The
16
17 reaction was performed in the temperature span of 100-180 °C. The effect of reaction time (1-
18
19 6 h), catalyst amount (0.15-1 g), and solvent (water/DMSO) were studied. All the reactions
20
21 were allowed to proceed for a specified time and after the reaction, the glass reactor was
22
23 quenched in cold water to stop the reaction immediately and centrifuged at 8000 rpm to
24
25 separate the catalyst. For all those reactions, where only water was used as a solvent, inside the
26
27 reactor, a little higher pressure than ambient might be possible during the reaction. However,
28
29 since the condenser top was open to the atmosphere, and proper cooling was maintained at the
30
31 top of the reactor, it was assumed that the reactions were operated at atmospheric pressure.
32
33
34
35
36
37
38
39
40
41
42
43
44
45
46
47
48
49
50
51
52
53
54
55
56
57
58
59
60

Product composition was identified and quantified in high-pressure liquid chromatography (HPLC, WATERS, 515, USA) furnished with a binary pump, HPX 87-H column (Bio-Rad Aminex, 4.6 mm × 350 mm, USA), and a RI detector (WATERS 2414, USA). During product analysis, the temperature of the HPLC column was adjusted with the help of a column heater. The detector and column temperatures were maintained at 35 °C and 60 °C, respectively. Before each analysis, dissolved oxygen present in the mobile phase (0.005 M H₂SO₄) was removed while stirring under vacuum. The flow rate of the mobile phase was maintained at 0.55 mL min⁻¹ and the injection volume in the HPLC was 20 μL. The product liquid was filtered with a syringe filter (0.22 μm) before each analysis. Standard calibration curves prepared for the individual compound was used to calculate the molar concentration of

reactant as well as products. Conversion and product yield were calculated by using the following equations.

$$\text{Conversion (\%)} = [(\text{moles converted} / \text{moles fed}) \times 100] \quad (1)$$

$$\text{Yield (\%)} = [(\text{moles of product} / \text{moles of reactant fed}) \times 100] \quad (2)$$

The retentate obtained after the separation of the catalyst from the reaction mixture by centrifuge were analyzed in an Ion chromatography (882 IC Plus-Anion, Metrohm, USA) equipped with Metrosep A Supp 5–250/4 ion-exchanged column and suppressed CD (J003) detector. The mobile phase was sodium carbonate (3.2 mmol/L) and sodium bicarbonate (1 mmol/L). The flow rate of the mobile phase was kept at 0.7 mL/min and the analysis time was 40 minutes, respectively.

3. Results and discussion

3.1 Catalyst characterization

3.1.1 BET

The obtained isotherms of catalysts are shown in Fig. 1. Distinctive type-IV isotherms with prominent H3 type hysteresis loop with a sharp descent at a comparative pressure of $0.7 < P/P_0 < 1$ are observed. This result established a regular mesoporous structure of catalysts.^{36–38} The obtained pore volume, average pore size, and surface area of TiO₂, and SO₄²⁻/TiO₂ are summarized in Table 1. The surface area of TiO₂ was highest (65 m² g⁻¹) and after incorporation of SO₄²⁻, it was decreased significantly, due to the aggregation of small crystallites and the blockage of pores by sulfate species.^{36,38–40} Huang et al.⁴¹ reported a ~ 60% reduction of the surface area of commercial TiO₂ after the treatment of 0.5 (M) H₂SO₄. Nakhate et al.³⁸ observed the reduction of surface area after sulfation of TiO₂. Lam et al.⁴⁰ prepared the SO₄²⁻/SnO₂ catalyst and reported the reduction of surface area after sulfation. However, the previously reported surface area for sulfated TiO₂ was different as compared to the values reported in Table 1. This variation was might be due to the use of different catalyst synthesis techniques.

The pore volume of the catalysts was also followed a similar trend as surface area. TiO_2 showed the highest pore volume of $0.24 \text{ cm}^3 \text{ g}^{-1}$ with respect to sulfated TiO_2 ($0.03\text{-}0.2 \text{ cm}^3 \text{ g}^{-1}$) (Table 1). The pore volume of the catalyst dropped because of the incorporation of sulfate on TiO_2 .³⁹ The obtained pore size of the catalyst was in the range of 12.6 - 18.2 nm.

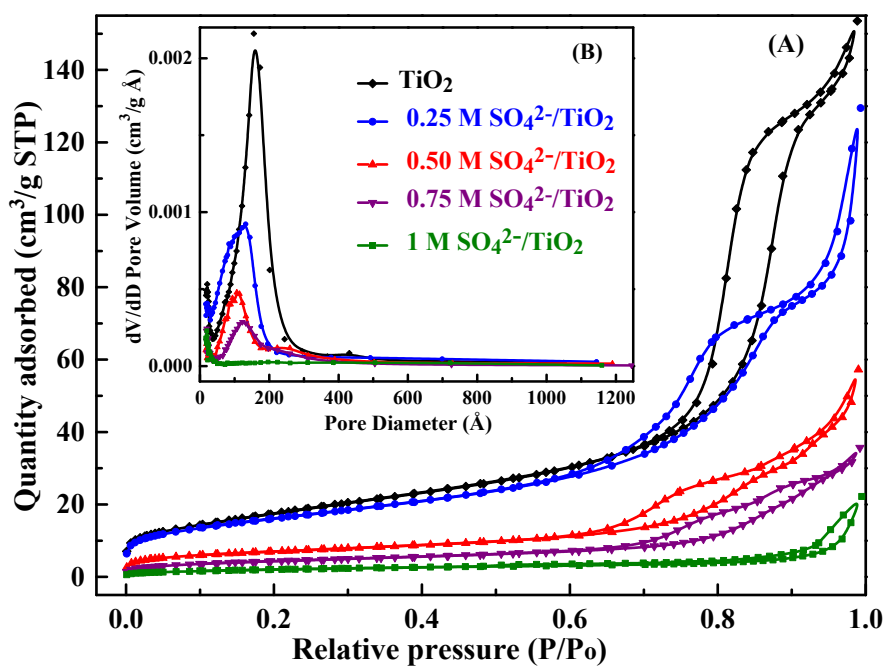


Fig. 1 (A) Nitrogen adsorption-desorption isotherm (B) Pore size distribution of catalyst.

Table 1 Physio-chemical properties of catalysts

Catalyst	BET surface area (m ² g ⁻¹)	Pore volume (cm ³ g ⁻¹)	Pore size (nm)	Average crystallite size (nm)	Acidic strength (mmol g ⁻¹ cat.)			Lewis (L) and Brønsted (B) sites strength (mmol g ⁻¹ cat.)		
					weak	medium	Total	L- sites	B-sites	B/L ratio
TiO ₂	65.0	0.24	12.6	14.0	0.027	0.035	0.06	0.039	0.056	1.43
0.25 M SO ₄ ²⁻ /TiO ₂	58.0	0.20	12.9	18.3	0.098	0.042	0.14	0.021	0.063	2.99
0.50 M SO ₄ ²⁻ /TiO ₂	24.7	0.09	13.2	20.3	0.031	0.538	0.57	0.027	0.237	8.81
0.75 M SO ₄ ²⁻ /TiO ₂	15.7	0.06	12.8	21.9	0.010	0.047	0.06	0.016	0.087	5.51
1 M SO ₄ ²⁻ /TiO ₂	7.5	0.03	18.2	22.8	0.008	0.029	0.04	0.012	0.055	4.41

3.1.2 X-ray diffraction (XRD)

View Article Online
DOI: 10.1039/D0NJ04151C

XRD patterns of TiO₂ and sulfated TiO₂ are shown in Fig. 2. For TiO₂, major diffraction peaks detected at the 2θ value of 25.3, 37.8, 48.2, 53.9, 55.1, 62.7, 68.9, 70.4, 75.3 and 82.6 represented (101), (112), (200), (105), (211), (204), (116), (220), (215) and (224) tetragonal TiO₂ anatase phase [JCPDS:21-1272].^{37,42,43} For sulfated TiO₂, additional peaks detected at the 2θ value of 16.2, 21.3, 22.2, 23.7, 27.6 and 28.2, corresponding to (020), (120), (101), (111), (121) and (200) crystal planes of TiO(SO₄) [JCPDS: 032-1372].³⁹ The peak intensity corresponding to TiO(SO₄) was found to be increased with increasing the SO₄²⁻ concentration in the catalysts. These results demonstrated the interactions between TiO₂ and sulfate species incorporated. Moreover, it was also observed that the intensity of the major peaks at the 2θ of 25.3 correspondings to the anatase (101) crystal plane of TiO₂ decreased significantly with increasing the sulfate concentration in the catalyst. This might be due to the distribution of the sulfate group on the surface of Titania.³⁷ A similar kind of observation for the sulfated TiO₂ catalyst is also reported by Dalai et al.⁴⁴ The obtained XRD patterns of sulfated TiO₂ (Fig. 2) demonstrated that with increasing the sulfate concentration in the catalysts, the tetragonal structure of the anatase phase of TiO₂ gradually transformed into the orthorhombic phase [JCPDS: 032-1372]. This phase transformation was prominently observed for the catalyst treated with a higher H₂SO₄ concentration (> 0.75 M). The average crystallite size of TiO₂ and sulfated TiO₂ were calculated by using the Scherrer formula from the line width of their relevant peaks detected at the 2θ value of 25.3, 37.9, 48.2, 53.9, 55.2, 62.7 and 16.2, 21.4, 22.1, 23.6, 25.3, 37.8, 48.2, 53.9, 55.2, 62.7, respectively. For TiO₂, the average crystallite size was found to be 14.0 nm (Table 1). For the sulfated TiO₂ these values were found to be increased, and it was in the range of 18.3-22.5 nm. With increasing the sulfate ion concentration, these values were also exhibited a marginal increasing trend. After impregnation and with increasing the sulfate amount, the particles get agglomerated and aggregated due to the electrostatic

interaction of sulfate ions. After the impregnation of SO_4^{2-} ion on TiO_2 , it replaced one O atom in O-Ti-O framework which increased the atomic radius.⁴² As a result, the particle size, pore-volume, and crystallite size of sulfated titania were increased. For sulfated titania, a similar type of result was also found by Niu et al.⁴²

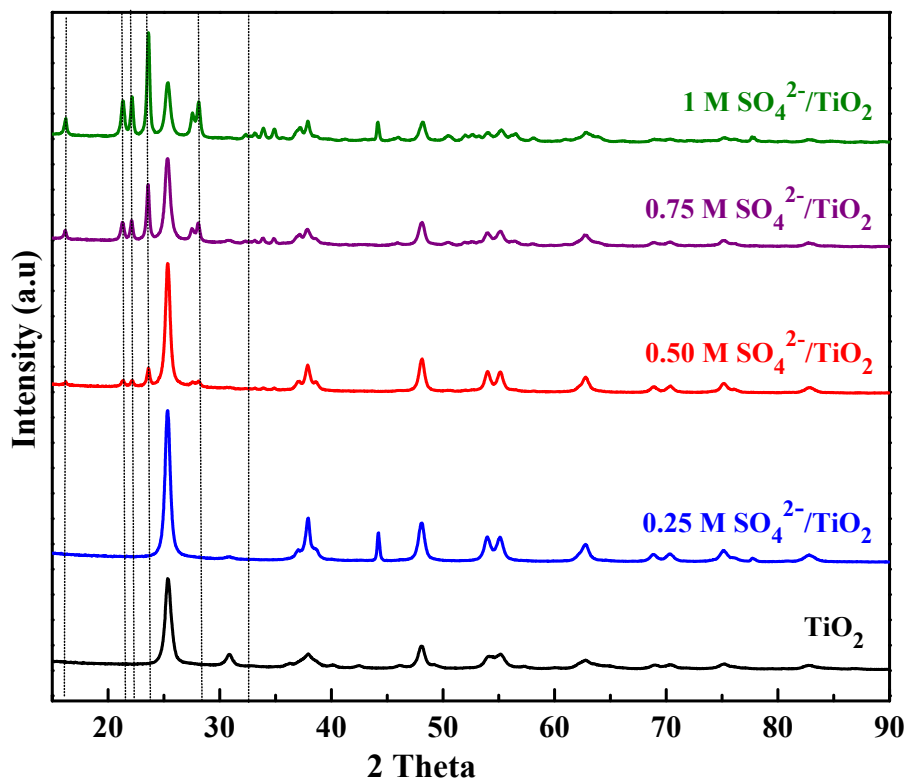


Fig. 2 XRD pattern of catalyst.

3.1.3 Thermo-gravimetric analysis (TGA)

The thermal stability of the catalysts was determined by TGA and the results obtained are shown in Fig. 3. For TiO_2 , minor weight loss was detected at < 200 °C, due to the removal of moisture⁴⁵. For sulfated catalysts, two steps weight loss was detected. Initial weight loss at < 200 °C was due to the dissipation of bound water and moisture, and another major weight loss observed at higher temperatures (550-800 °C) was due to the decomposition of sulfate.^{39,45-48} The high-temperature wet loss was found to be increased from 1.4 to 32.5%, with increasing the sulfate concentration in the catalyst (Fig. 3(A)-(E)). It was also observed that higher

temperature weight loss for sulfated TiO_2 shifted gradually towards higher temperature side with increasing the SO_4^{2-} concentration. Gardy et al.³⁹ reported two steps weight losses for the titania nanocatalyst due to moisture and sulfate decomposition in the temperature range of 50-200 °C and 600-800 °C, respectively. The observed weight loss due to sulfate decomposition was ~47% at 600-800 °C. Bai et al.⁴⁸ explained the weight loss due to sulfate decomposition at >500 °C, which also collapsed the porous channel of sulfated TiO_2 . Sulfated Titania catalyst synthesized by hydrolysis of titanium oxysulfate was found to be stable up to 500 °C.⁴⁶ The obtained TGA results in this study depicted that calcination of this catalyst at 550 °C and higher will affect the acidic strength of the catalyst due to sulfate decomposition.⁴⁶

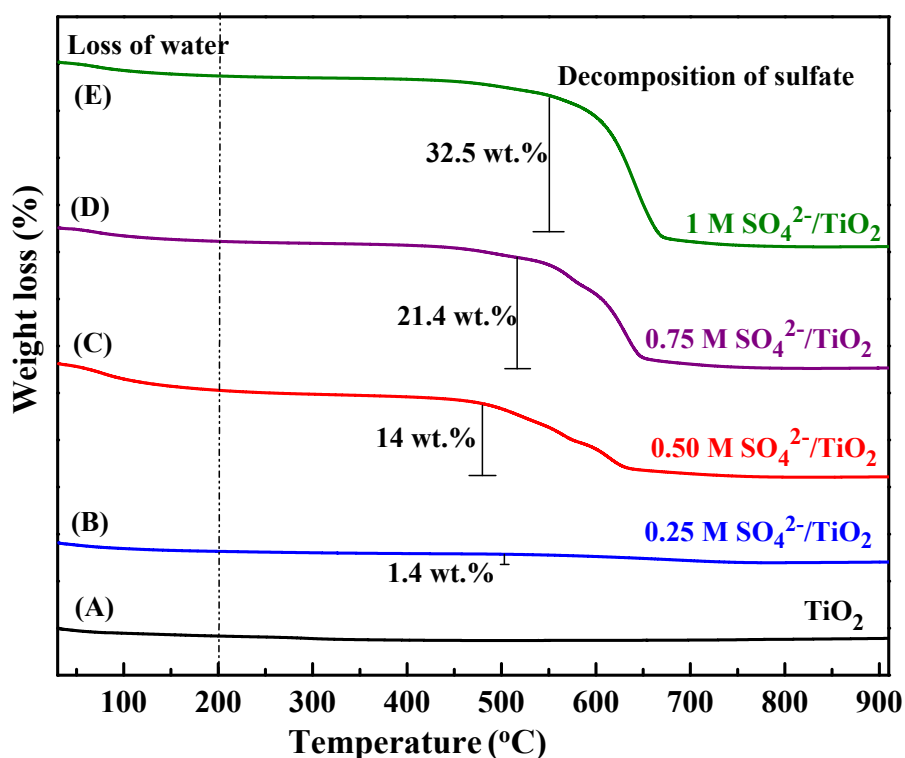


Fig. 3 TGA profile of catalyst.

3.1.4 Morphology

Surface morphology and elemental composition of TiO_2 and sulfated TiO_2 catalysts determined by FE-SEM with EDX and TEM analysis, respectively. In the SEM image of TiO_2

(Fig. 4(A)), uniformly distributed spherical particles were detected. After the addition of the sulfate group in TiO_2 , small spherical particles were found to be agglomerated [Fig. 4(B)] and bigger clusters were formed at higher sulfate concentrations [> 0.5 (M)] (Fig. 4(B)-(E)). The aggregation of particles might be due to an electrostatic attraction among the sulfate ions.^{39,49}

Furthermore, FE-SEM equipped with EDX was used to analyze the elemental compositional of the catalysts. The presence of titanium, oxygen, and sulfur in the catalysts was confirmed by SEM-EDX as shown in Fig. (4(A)-(E)). TiO_2 exhibited two major peaks at around 4.5 keV and 5 keV, respectively. The intense peak obtained at 4.5 keV corresponding to the bulk TiO_2 and the less intense peak detected at 5 keV was assigned for surface TiO_2 .^{50,51} The peak corresponding to sulfur was visible at around 2.25 keV (Fig. 4(B)-(E)). In addition to that, uniformly distributed sulfate on the catalyst was confirmed from the elemental mapping of 0.5 M $\text{SO}_4^{2-}/\text{TiO}_2$ catalyst (Fig. 4(E)). The obtained TEM and SAED images of 0.5 M $\text{SO}_4^{2-}/\text{TiO}_2$ catalyst are shown in Fig. 4(F). In the TEM image of 0.5 M $\text{SO}_4^{2-}/\text{TiO}_2$ catalyst, similar spherical morphology of the particles was observed as SEM. The measured particle sizes were in the range of 15-20 nm (inserted histogram in Fig. 4(F)), which agreed very well with the mean crystallite size (20.3 nm) deliberated by XRD. The polycrystalline structure of the catalyst was confirmed from the SAED pattern obtained. As shown in Fig. 4(F), rings of the bright spots were detected and each spot arises from the Bragg's reflection from their crystallite planes.

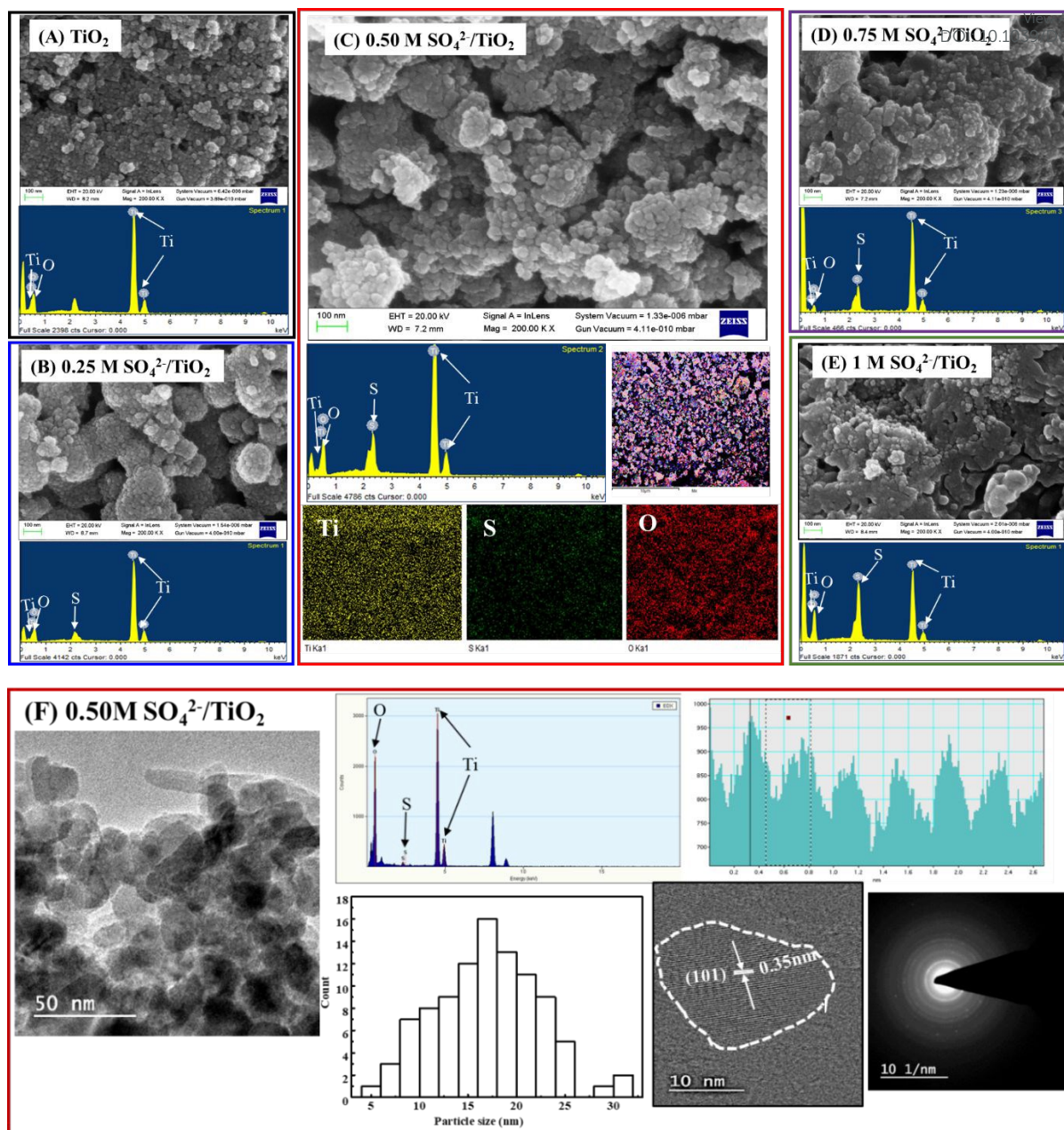


Fig. 4 FE-SEM image of catalyst (A) TiO₂ with EDX (B) 0.25 M SO₄²⁻/TiO₂ with EDX (C) 0.50 M SO₄²⁻/TiO₂ with EDX and electron mapping of Ti, S, O (D) 0.75 M SO₄²⁻/TiO₂ with EDX (E) 1 M SO₄²⁻/TiO₂ with EDX (F) HR-TEM image of 0.50 M SO₄²⁻/TiO₂ with SAED image and lattice fringes of TiO₂ and particle size histogram. (All the FESEM images are taken at 100 nm scale and 200.00 K X magnification. The EDAX scale is from 0 to 10 keV for all the FESEM-EDAX images.)

3.1.5 Acidic strength

View Article Online
DOI: 10.1039/D0NJ04151C

The comprehensive acidic strength of catalysts was measured by temperature-programmed desorption (TPD) analysis. TPD was performed up to 1000 °C (Fig. 5(A)), however, the peak detected at 550 °C and higher were not considered for calculation because these peaks represented sulfate decomposition as confirmed by TGA (Fig. 3). As shown in Fig. 5(A), for all the catalysts, ammonia desorption peaks were observed primarily in two different temperature regions. Peaks obtained in the lower temperature region (50-300 °C) represented the weak acidic sites and the peaks detected at higher temperatures (> 300 °C) attributed to medium strength acidic sites.⁵² The total acidic strength of the catalyst was estimated based on the total amount of ammonia desorbed and detected by TCD (Table 1). The total integral area of the NH₃ desorption curve represented the amount of ammonia adsorbed (STP g⁻¹) at different temperatures. It can be seen from Fig. 5(A) that sulfated catalyst displayed weak and medium strength acidic sites and the highest total acidic strength of 0.57 mmol g⁻¹ cat. was obtained for 0.5 M SO₄²⁻/TiO₂. On further increasing the sulfate loading (> 0.5 M), this value decreased significantly. This decrease in acidic strength might be due to the formation of polysulfate.⁵³ The gradual shifting of the TPD peak towards higher temperatures was also observed with increasing the sulfate concentration in TiO₂. This temperature shift indicated some monotonic increase in the average acidic strength of catalyst with increasing the sulfate concentration.⁴⁴

Lewis and Brønsted acid sites on the TiO₂ and SO₄²⁻/TiO₂ catalyst characterized by pyridine-FTIR (Fig. 5(B)). Pyridine absorption peaks detected at the wavenumber of 1443 cm⁻¹ and 1484 cm⁻¹ represented the Lewis and Brønsted acid sites, respectively, whereas the absorbance peak at ~1535 cm⁻¹ demonstrated the combined Lewis and Brønsted acid sites.¹ The vibrational band detected at ~1639 cm⁻¹ represented the hydrogen-bonded pyridine.³¹ The ratio of Brønsted/Lewis acid strength on the catalyst surface was calculated by following a standard method described elsewhere.³⁵ The integral area of the respective absorbance peaks

detected was considered for calculation. The ratio of Brønsted/Lewis acidic strength on the catalyst was found to be increased with sulfate concentration up to 0.5 (M), and the maximum ratio of 8.81 was obtained (Table 1). Further increasing the sulfate loading on the catalyst, this ratio decreased due to the morphological changes of the catalyst surface treated with concentrated H_2SO_4 acid. These results revealed a good agreement with the NH_3 -TPD data.

The presence of both the Brønsted and Lewis acidic sites on TiO_2 is also reported earlier. Bezrodna et al.⁵⁴ investigated pyridine- TiO_2 surface interaction as a probe for surface active center analysis and reported the presence of both the acidic sites on the TiO_2 surface. It was demonstrated that the availability of hydroxyls groups on the TiO_2 surface was responsible for the Brønsted acidity. Li et al.⁵⁵ also confirmed the presence of both Brønsted and Lewis sites on the TiO_2 surface in their study on the synthesis and characterization of TiO_2 polymorphs. In this study, in the FTIR of TiO_2 (Figure 7) the O-H, H-O-H, and Ti-O stretching were detected at the Web number of 3414.8 cm^{-1} , 1635.5 cm^{-1} , and $500\text{-}700\text{ cm}^{-1}$, respectively. These results supported the presence of the O-H group on the TiO_2 surface which was responsible for Brønsted acidity.

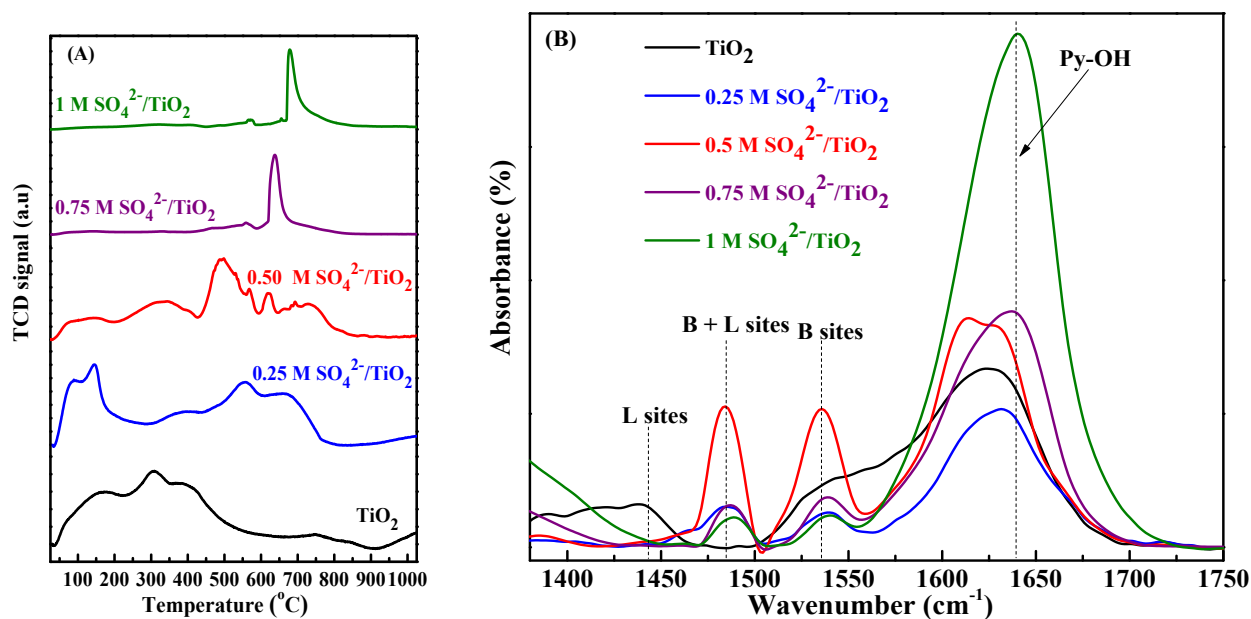


Fig. 5 (A) TPD profile of catalyst, (B) Pyridine-FTIR spectra of TiO_2 , 0.25 M $\text{SO}_4^{2-}/\text{TiO}_2$, 0.5 M $\text{SO}_4^{2-}/\text{TiO}_2$, 0.75 M $\text{SO}_4^{2-}/\text{TiO}_2$, and 1 M $\text{SO}_4^{2-}/\text{TiO}_2$ at room temperature.

3.1.6 X-ray photoelectron spectrum (XPS)

High-resolution XPS spectrum survey scans of TiO_2 , and 0.5 M $\text{SO}_4^{2-}/\text{TiO}_2$ catalysts are shown in Fig. 6. As shown in Fig. 6(A), four significant XPS peaks respective to S 2p, C 1s, Ti 2p, and O 1s are observed at 164.8 eV, 284.7 eV, 458 eV, and 531 eV binding energy, respectively. In the entire spectra, C 1s peak was allied to the hydrocarbon species present in the XPS instrument itself. However, the XPS spectra detected at the binding energy of 458.4 eV and 464.3 eV corresponded to Ti 2p_{3/2} and Ti 2p_{1/2} of Ti 2p of pure TiO_2 . These characteristic XPS spectra represented the anatase phase of TiO_2 as reported earlier.⁵⁶ For TiO_2 , the spin-orbital splitting of 5.7 eV revealed a +4 oxidation state of titanium in the lattice.^{39,57,58} For 0.5 M $\text{SO}_4^{2-}/\text{TiO}_2$ catalyst, the peaks corresponding to Ti 2p_{1/2} and Ti 2p_{3/2} shifted slightly towards higher binder energy i.e., at 459.2 eV, and 464.9 eV, respectively. This result indicated the interaction between the sulfate group and Titania in the catalyst (Fig. 6(B)). However, the spin-orbit splitting value was found to be unchanged (5.7 eV), which indicated the +4 oxidation state of titanium in the 0.5 M $\text{SO}_4^{2-}/\text{TiO}_2$ catalyst. The major peak at the binding energy of 529.7 eV corresponded to the O-Ti-O bond,^{46,56} and the shoulder peak at the 531.1 eV might be due to the O-H bond of the chemisorbed water molecule present on the catalyst surface.^{36,37,49} For the sulfated catalyst, the peaks corresponding to O 1s shifted towards higher binding energy (0.7-0.8 eV) (Fig. 6C). The peaks at 530.4 eV were due to the Ti-O-S bond,^{46,56} and the second peak at 531.9 eV was due to the O-S bond of sulfate group and/or O-H bond and chemisorbed water molecules, respectively.^{36,37,49} For all the catalysts, the XPS spectra of S 2p were de-convoluted into two peaks by Gaussian fitting (Fig. 6(D)). Finally, the peaks detected at the binding energy of ~169 eV for S 2p were de-convoluted into two different peaks at 168.9 eV and 169.7 eV which represented S 2p_{1/2} and S 2p_{3/2}, respectively. This S 2p

peaks confirmed the presence of sulfate group on TiO_2 . Similar kind of metal sulfate integrations is reported by Niu et al.⁴²

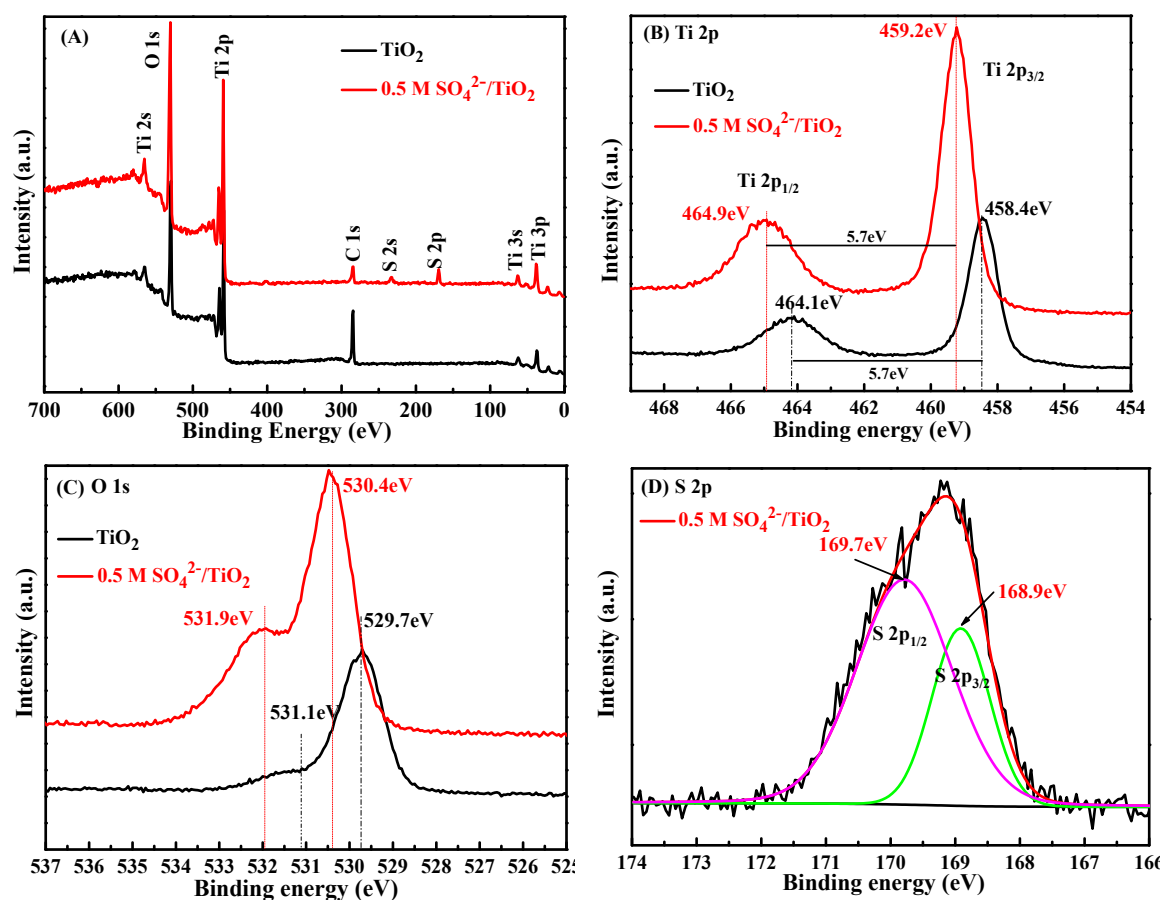


Fig. 6 (A) Survey scan XPS spectra of TiO_2 , $0.5 \text{ M SO}_4^{2-}/\text{TiO}_2$, (B) Ti 2p, (C) O 1s, and (d) S 2p.

3.1.7 Fourier transform infrared spectroscopy (FT-IR)

Fig. 7 presents the FT-IR spectra of TiO_2 and $0.5 \text{ M SO}_4^{2-}/\text{TiO}_2$ catalysts. For TiO_2 , four major stretching vibrational bands were detected at the wavenumber of 3414.8 cm^{-1} , 2356.7 cm^{-1} , 1635.5 cm^{-1} , and $500\text{-}700 \text{ cm}^{-1}$, respectively. A strong wide band at the wavenumber of 3414.8 cm^{-1} was due to O-H stretching of water molecule adsorbed on the TiO_2 surface.^{37,39,42,48} The vibration stretching detected at 2356.7 cm^{-1} wavenumber was corresponding to the O=C=O stretching of CO_2 molecule adsorption from the air.³⁹ However, H-O-H symmetric vibration of adsorbed water molecules was detected at the wavenumber of

1635.5 cm^{-1} . The band at 557 cm^{-1} and 667.5 cm^{-1} wavenumbers represented the characteristics of vibrational stretching of the Ti-O bond.

In the FT-IR spectra of 0.5 M $\text{SO}_4^{2-}/\text{TiO}_2$ catalyst additional four peaks were detected in the wavenumber range of 900-1300 cm^{-1} (Fig. 7). The absorption bands detected in the region of 1130-1240 cm^{-1} , were assigned to S=O vibration stretching.⁵⁹ The strong band at 1047.8 cm^{-1} and 987 cm^{-1} were related to S-O stretching which was assigned to chelating bidentate SO_4^{2-} coordination with Ti^{4+} .^{59,60} These results are in good agreement with XPS results which manifested a strong predominance of SO_4^{2-} ions at the surface of the sulfated catalyst.

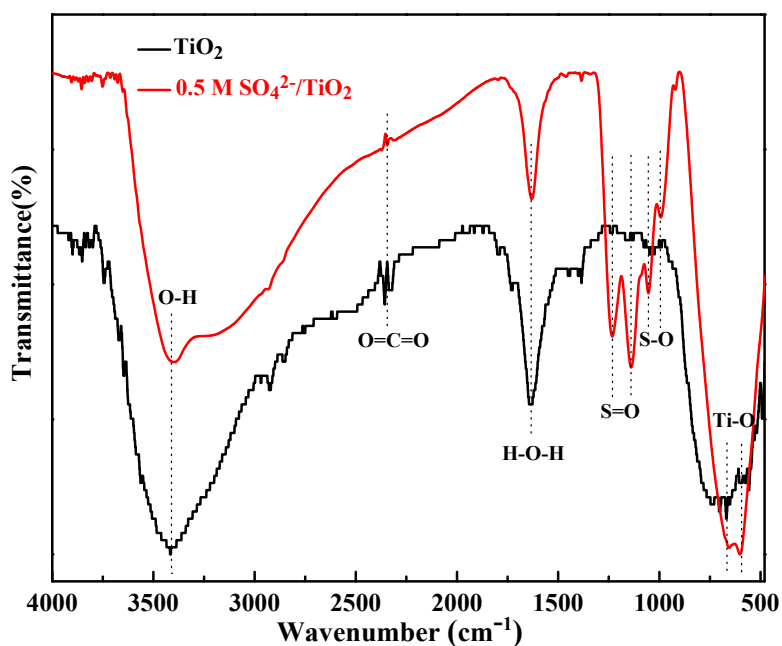


Fig. 7 FTIR spectra of TiO_2 , and 0.5 M $\text{SO}_4^{2-}/\text{TiO}_2$ at room temperature.

3.2 Catalytic performance

Initially, the dehydration ability of TiO_2 and 1 M $\text{SO}_4^{2-}/\text{TiO}_2$ catalyst was evaluated at standard reaction conditions.¹⁷ To verify the homogeneous reaction, a blank run was performed in absence of a catalyst, and it was demonstrated ~32.6% conversion of glucose, and the main products including 5-hydroxymethylfurfural, levulinic acid, formic acid were not detected in

the product mixture (Fig. 8). At this condition, glucose was converted to some other unknown unidentified compounds. The HPLC chromatogram of the products is given in the supplementary file (Fig. S1). However, in presence of a catalyst, the major reaction products were 5-HMF, LA, FA, and black organic polymer might be humin.²⁷ The black organic polymer (soluble and insoluble) might be formed due to the condensation reaction of glucose, fructose, 5-HMF, and other intermediates in the presence of high acidity of the catalyst. Dehydration of glucose followed the reaction path as shown in Fig. 9.³⁵ In presence of TiO₂ catalysts, glucose conversion, and the yield of 5-HMF, LA, FA was 74.7%, 14%, 4.4%, and 5%, respectively (Fig. 8). For 1 M SO₄²⁻/TiO₂ catalyst, glucose conversion was further increased to 98.4%, and the yield 5-HMF, LA, and FA was 31.8%, 4.8%, and 11.5%, respectively. An almost 2.2-fold increase of 5-HMF yield was observed with 1 M SO₄²⁻/TiO₂ catalyst as compared to pure TiO₂. The appearance of Brønsted acid centers after the addition of sulfate ions in TiO₂ was the primary reason for higher dehydration activity, which also promoted the yield of 5-HMF. The presence of both Lewis and Brønsted acid sites on the catalyst surface derived the glucose dehydration reaction as reported earlier.⁸ A decent yield (31.8%) of 5-HMF was higher as compared to the results reported in the previous literature in the DMSO medium. Yan et al. reported a 19.2% 5-HMF yield at 95.2% glucose conversion over sulfated zirconia catalyst at 140 °C and after 4 h.¹⁸ Feng et al. achieved a 25.8% yield of 5-HMF with SO₄²⁻/ZrO₂ modified H⁺ zeolite catalyst at 195 °C after 90 min.²⁸ Since the sulfated TiO₂ performed better as compared to pure TiO₂ in terms of glucose dehydration to 5-HMF, therefore, the effect of sulfate concentration on TiO₂ catalysts was investigated and the reaction variables were optimized for higher 5-HMF yield, which is discussed in the following sections.

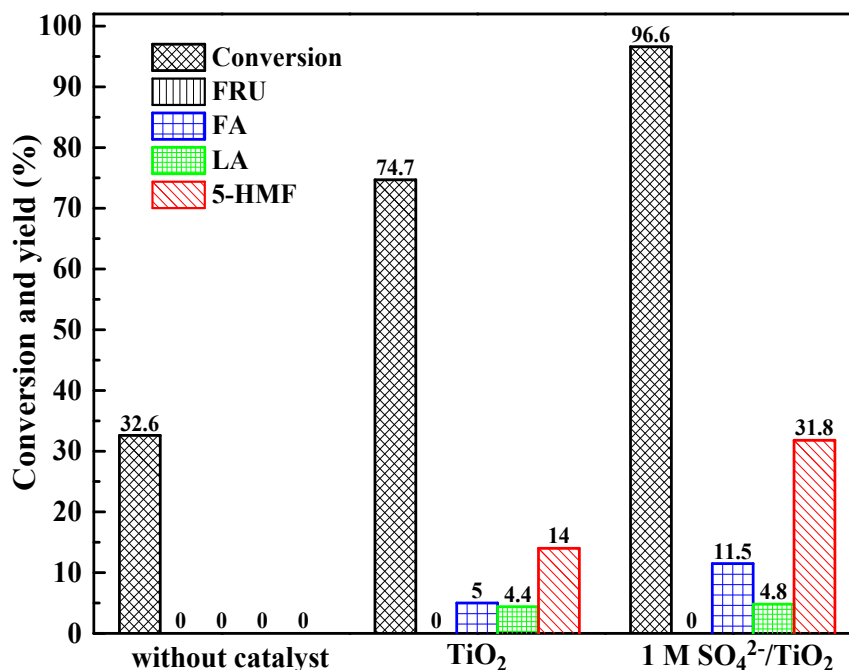


Fig. 8 Performance of various catalysts on glucose dehydration to 5-HMF.

Reaction condition: 1 g glucose, 0.5 g catalyst, 10 mL DMSO, 150 °C, 6 h.

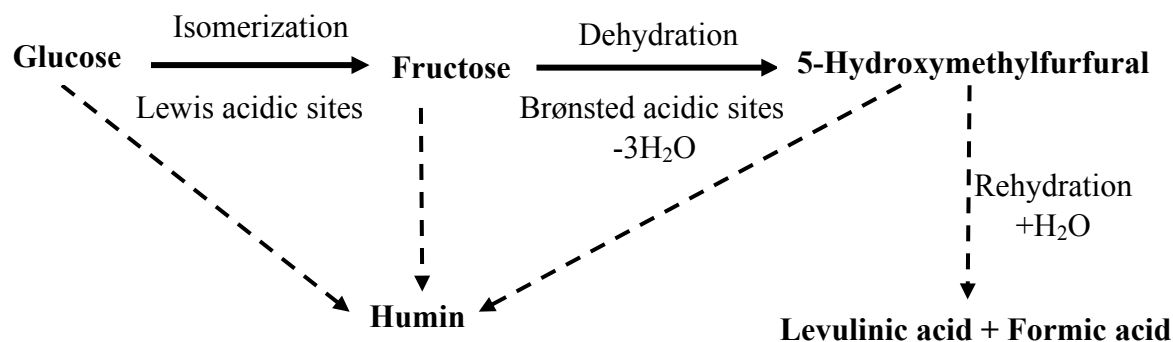


Fig. 9 Reaction pathways of glucose dehydration.

3.2.1 Effect of temperature and time on conversion of glucose to 5-HMF

The effect of reaction temperature on glucose conversion and product yields are shown in Fig. 10(A). The temperature was deviated in the span of 100-180 °C by keeping other reaction parameters constant and the experimental data were collected after a run time of 6 h. The temperature effect on glucose conversion was found to be very significant and it increased from 11.7% at 100 °C to 100% at 180 °C. In the entire temperature domain, 5-HMF, LA, and

1
2
3 FA were found to be the major reaction products. As reported in the previous literature, 5-HMF Article Online
DOI: 10.1059/NJ04151C
4
5 has formed via two-step dehydration of glucose i.e. glucose to fructose followed by fructose to
6
7 5-HMF. In this study, fructose was not detected, which indicated the faster dehydration of
8
9 fructose in presence of 1 M $\text{SO}_4^{2-}/\text{TiO}_2$ catalyst having both Lewis and Brønsted acid sites.
10
11 The yield of 5-HMF passed through maxima at ~ 150 °C, and at higher temperatures, 5-HMF
12
13 degraded to other side products such as FA and organic polymers. At higher temperatures
14
15 (typically >150 °C), the formation of the soluble and insoluble dark color compounds was
16
17 observed. Fig. 10(B) showing the gradual color variation of the reaction medium with
18
19 temperature. These organic polymers are formed due to the degradation of glucose as well as
20
21 other primary glucose dehydration products via side reactions.²³ The highest 5-HMF yield of
22
23 $\sim 32\%$ was obtained at 150 °C.

24
25
26
27
28
29
30
31
32
33
34
35
36
37
38
39
40
41
42
43
44
45
46
47
48
49
50
51
52
53
54
55
56
57
58
59
60
61
62
63
64
65
66
67
68
69
70
71
72
73
74
75
76
77
78
79
80
81
82
83
84
85
86
87
88
89
90
91
92
93
94
95
96
97
98
99
100
101
102
103
104
105
106
107
108
109
110
111
112
113
114
115
116
117
118
119
120
121
122
123
124
125
126
127
128
129
130
131
132
133
134
135
136
137
138
139
140
141
142
143
144
145
146
147
148
149
150
151
152
153
154
155
156
157
158
159
160
161
162
163
164
165
166
167
168
169
170
171
172
173
174
175
176
177
178
179
180
181
182
183
184
185
186
187
188
189
190
191
192
193
194
195
196
197
198
199
200
201
202
203
204
205
206
207
208
209
210
211
212
213
214
215
216
217
218
219
220
221
222
223
224
225
226
227
228
229
230
231
232
233
234
235
236
237
238
239
240
241
242
243
244
245
246
247
248
249
250
251
252
253
254
255
256
257
258
259
260
261
262
263
264
265
266
267
268
269
270
271
272
273
274
275
276
277
278
279
280
281
282
283
284
285
286
287
288
289
290
291
292
293
294
295
296
297
298
299
300
301
302
303
304
305
306
307
308
309
310
311
312
313
314
315
316
317
318
319
320
321
322
323
324
325
326
327
328
329
330
331
332
333
334
335
336
337
338
339
340
341
342
343
344
345
346
347
348
349
350
351
352
353
354
355
356
357
358
359
360
361
362
363
364
365
366
367
368
369
370
371
372
373
374
375
376
377
378
379
380
381
382
383
384
385
386
387
388
389
390
391
392
393
394
395
396
397
398
399
400
401
402
403
404
405
406
407
408
409
410
411
412
413
414
415
416
417
418
419
420
421
422
423
424
425
426
427
428
429
430
431
432
433
434
435
436
437
438
439
440
441
442
443
444
445
446
447
448
449
450
451
452
453
454
455
456
457
458
459
460
461
462
463
464
465
466
467
468
469
470
471
472
473
474
475
476
477
478
479
480
481
482
483
484
485
486
487
488
489
490
491
492
493
494
495
496
497
498
499
500
501
502
503
504
505
506
507
508
509
510
511
512
513
514
515
516
517
518
519
520
521
522
523
524
525
526
527
528
529
530
531
532
533
534
535
536
537
538
539
540
541
542
543
544
545
546
547
548
549
550
551
552
553
554
555
556
557
558
559
560
561
562
563
564
565
566
567
568
569
570
571
572
573
574
575
576
577
578
579
580
581
582
583
584
585
586
587
588
589
590
591
592
593
594
595
596
597
598
599
600
601
602
603
604
605
606
607
608
609
610
611
612
613
614
615
616
617
618
619
620
621
622
623
624
625
626
627
628
629
630
631
632
633
634
635
636
637
638
639
640
641
642
643
644
645
646
647
648
649
650
651
652
653
654
655
656
657
658
659
660
661
662
663
664
665
666
667
668
669
670
671
672
673
674
675
676
677
678
679
680
681
682
683
684
685
686
687
688
689
690
691
692
693
694
695
696
697
698
699
700
701
702
703
704
705
706
707
708
709
710
711
712
713
714
715
716
717
718
719
720
721
722
723
724
725
726
727
728
729
730
731
732
733
734
735
736
737
738
739
740
741
742
743
744
745
746
747
748
749
750
751
752
753
754
755
756
757
758
759
760
761
762
763
764
765
766
767
768
769
770
771
772
773
774
775
776
777
778
779
780
781
782
783
784
785
786
787
788
789
790
791
792
793
794
795
796
797
798
799
800
801
802
803
804
805
806
807
808
809
810
811
812
813
814
815
816
817
818
819
820
821
822
823
824
825
826
827
828
829
830
831
832
833
834
835
836
837
838
839
840
841
842
843
844
845
846
847
848
849
850
851
852
853
854
855
856
857
858
859
860
861
862
863
864
865
866
867
868
869
870
871
872
873
874
875
876
877
878
879
880
881
882
883
884
885
886
887
888
889
890
891
892
893
894
895
896
897
898
899
900
901
902
903
904
905
906
907
908
909
910
911
912
913
914
915
916
917
918
919
920
921
922
923
924
925
926
927
928
929
930
931
932
933
934
935
936
937
938
939
940
941
942
943
944
945
946
947
948
949
950
951
952
953
954
955
956
957
958
959
960
961
962
963
964
965
966
967
968
969
970
971
972
973
974
975
976
977
978
979
980
981
982
983
984
985
986
987
988
989
990
991
992
993
994
995
996
997
998
999
1000

Significant amounts of 5-HMF rehydration products such as LA and FA were also formed and their concentrations varied with the variation of reaction temperature. The yield of LA increased from 2.1% to 4.9% at 150 °C and further it decreased at higher temperatures. Up to 140 °C, the yield of FA was negligible, after that the yield of FA was found to increase linearly with simultaneous decreasing the yield of 5-HMF as well as LA. These results demonstrated the formation of FA due to the rehydration of 5-HMF at higher temperatures ¹¹. The maximum FA yield of 38.7% was detected at 180 °C. At higher temperatures, the color of the reaction mixture became dark brown or black due to the more production of organic polymers which also supported the rehydration of 5-HMF as well as condensation of glucose to organic polymers at a higher temperature (Fig. 10(B)). The temperature effect study suggested that higher reaction temperature (>150 °C) favored the undesirable side reactions.

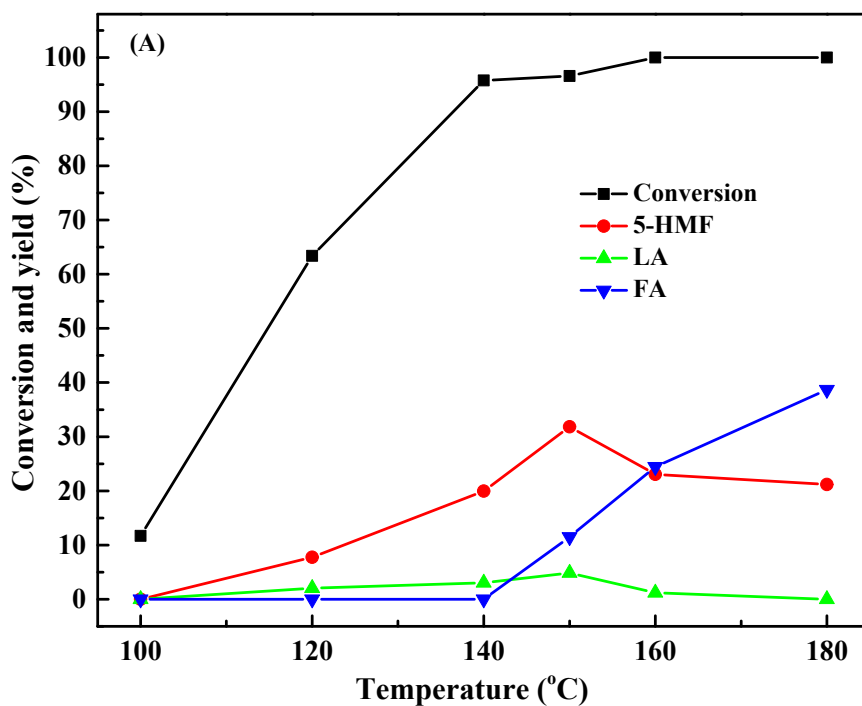


Fig. 10 (A) Effect of reaction temperature on glucose dehydration to 5-HMF.

Reaction condition: 1 g glucose, 0.5 g 1 M $\text{SO}_4^{2-}/\text{TiO}_2$ catalyst, 10 mL DMSO, 6 h



(I) (II) (III) (IV) (V) (VI)

Fig. 10 (B) Color of reaction mixture at temperature (I) 100 °C (II) 120 °C (III) 140 °C (IV) 150 °C (V) 160 °C (VI) 180 °C.

Fig. 11 shows the time effect on glucose conversion and the variation of product yield at 150 °C. Very high glucose conversion of ~80.5% was achieved even after 1 h, and it was > 98% after 5 h. These results suggested that the glucose dehydration rate was faster at 150 °C.

A similar kind of dehydration rate also reported by Teimouri et al.⁶¹ The 5-HMF yield was found to be increased with time and the maximum yield of 32.8% was achieved after 6 h, further it decreased at a slower rate. The formation of other rehydrated products such as FA, LA, and organic polymers was the primary reason for declining the yield of 5-HMF. Similar kinds of phenomena were also observed by several authors.³² Therefore, higher reaction time was not favorable for a greater 5-HMF yield. The obtained LA and FA yield were in the range of 1.5-4.9% and 6.9–13%, respectively.

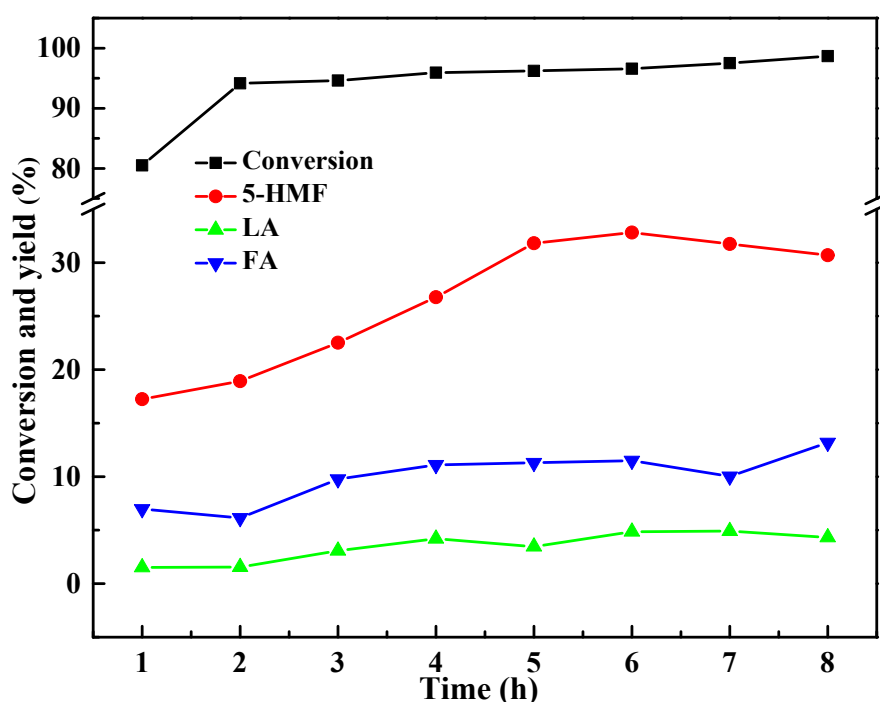


Fig. 11 Effect of reaction time on glucose dehydration to 5-HMF.

Reaction condition: 1 g glucose, 0.5 g 1 M $\text{SO}_4^{2-}/\text{TiO}_2$ catalyst, 10 mL DMSO, 150 °C.

3.2.2 Effect of catalyst amount

The role of catalyst amounts (0.15-1 g) was evaluated at 150 °C, and the products were analyzed after a run time of 6 h. As shown in Fig. 12, initially with increasing the catalyst amounts glucose conversion, as well as 5-HMF yield, increased due to increasing the accessibility of more active sites. A maximum of 32.8% 5-HMF yield was obtained with 0.5 g of catalyst and a further increase in catalyst amount yield decreased. The accessibility of more

active centers facilitated the rehydration of 5-HMF as well as other side reactions. Therefore,

0.5 g catalyst was considered as optimum.

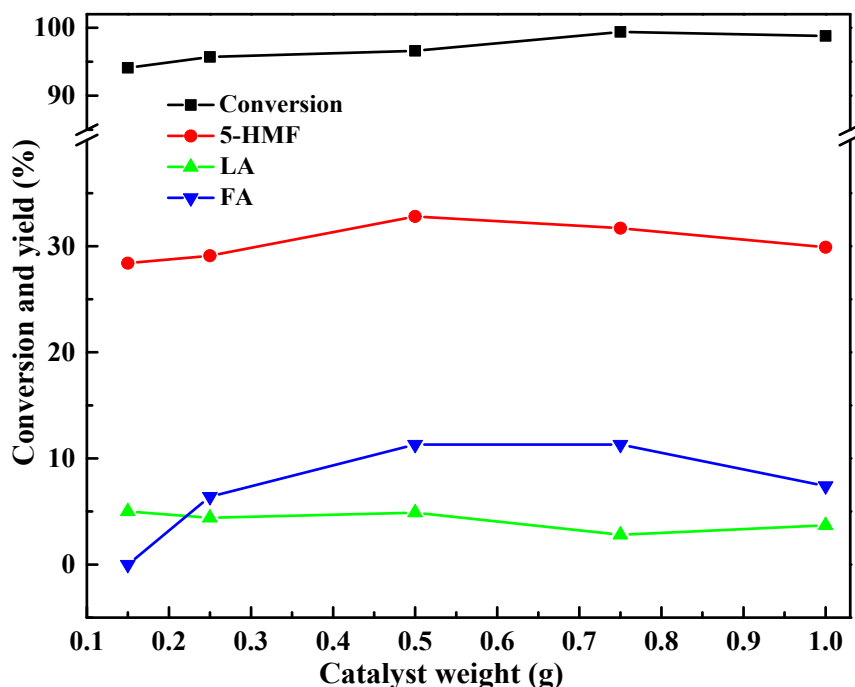
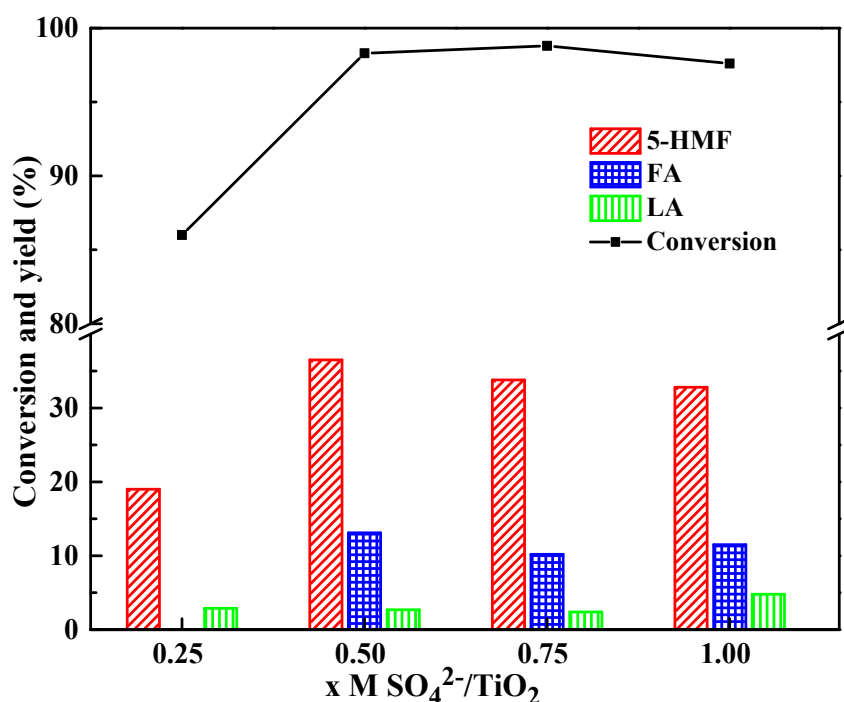


Fig. 12 Effect of catalyst amount on glucose dehydration to 5-HMF.

Reaction condition: 1 g glucose, 1 M $\text{SO}_4^{2-}/\text{TiO}_2$ catalyst, 10 mL DMSO, 150 °C, and 6 h.

3.2.3 Sulfate loading effect on TiO_2

The sulfate group was induced on titania to enrich the Brønsted acidic strength of the catalyst. Various Titania catalyst was prepared by treating the catalyst sample with H_2SO_4 of various molarity [0.25 (M)-1(M)], and their performance was evaluated at 150 °C. A maximum of 98.3% glucose conversion and ~37% 5-HMF yield were achieved in presence of titania catalyst treated with 0.5 (M) H_2SO_4 (Fig. 13). On further increment of the sulfate concentration (> 0.5 (M)), no significant increase in glucose conversion and 5-HMF yield were identified. It might be due to the saturation of the sulfate group on the titania surface beyond 0.5 (M).



View Article Online
DOI: 10.1039/D0NJ04151C

Fig. 13 Effect of sulfate loading on glucose dehydration reaction.

Reaction condition: 1 g glucose, 0.5 g, 10 mL DMSO, 150 °C, 6 h

3.2.4 Effect of water content on the conversion of glucose to 5-HMF

As shown in previous literature, water demonstrated a negative effect on the yield of 5-HMF.²⁴ The effect of water content in the DMSO medium on glucose conversion and 5-HMF yield was verified. With increasing water vol.%, the yield of 5-HMF was found to be decreased, and the maximum yield of ~37% was obtained when pure DMSO was used (Fig. 14). In the organic medium, during glucose dehydration, the water molecule produced is separated from the organic DMSO medium due to immiscibility, which facilitated more and more dehydration of glucose to 5-HMF. Therefore, the organic medium was good for the dehydration of glucose to 5-HMF.

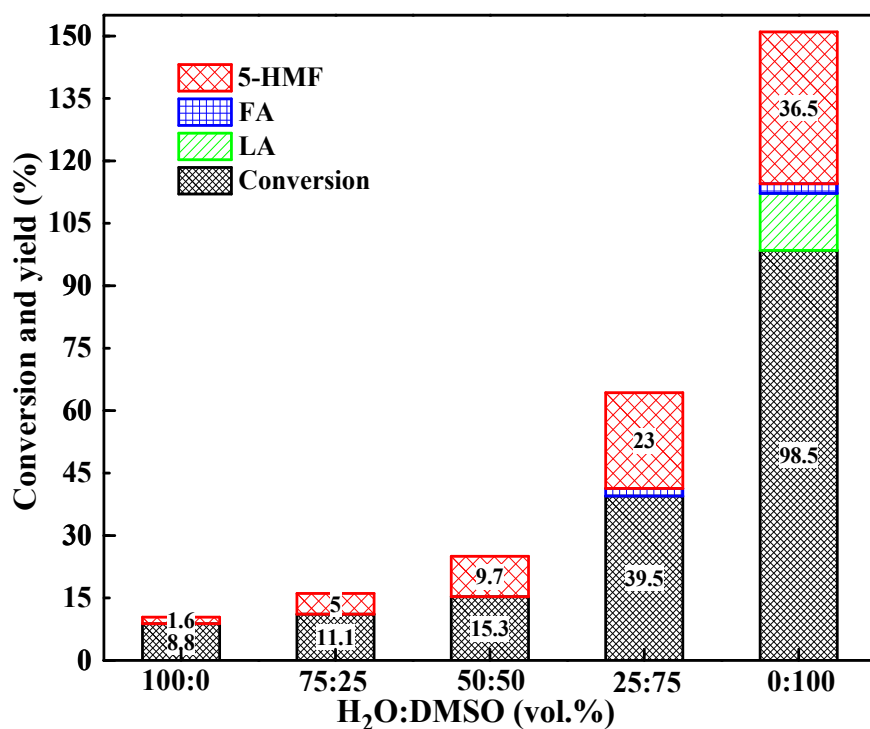
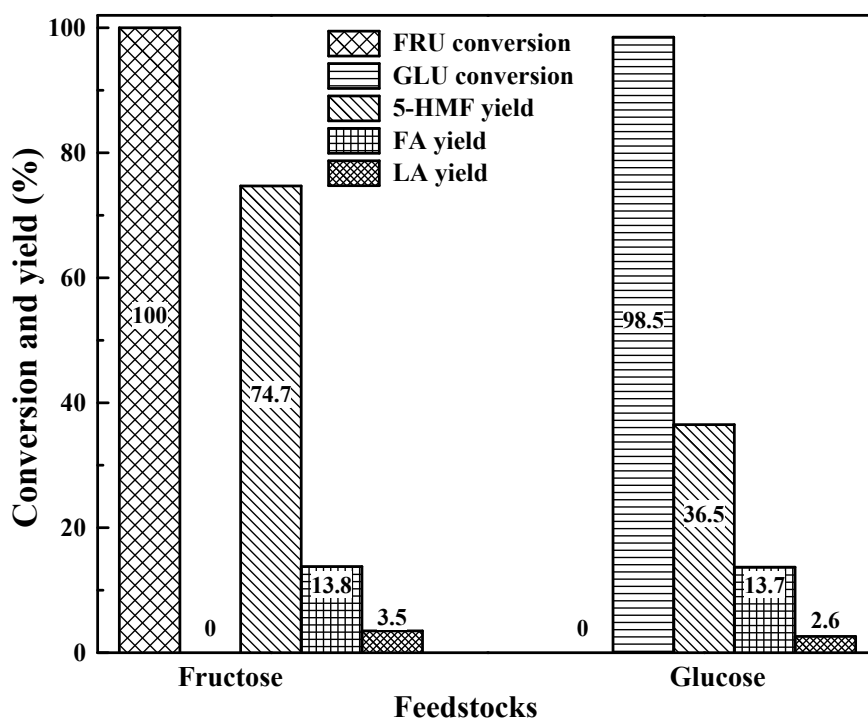
View Article Online
DOI: 10.1039/D0NJ04151C

Fig. 14 Effect of water amount (vol. %, in DMSO) on glucose dehydration to 5-HMF. Reaction condition: 1 g glucose, 0.5 g catalyst, 150 °C, 6 h.

3.2.5 Effect of feedstock

Fructose dehydration was performed in presence of 0.5 M $\text{SO}_4^{2-}/\text{TiO}_2$ catalyst at the optimum reaction condition obtained for glucose dehydration reaction and the results obtained are compared in Fig. 15. For both the feedstock, the conversion was almost 100%, however, the 5-HMF yield was significantly higher (74.7%) in presence of fructose as a feedstock. The lower yield of 5-HMF in presence of glucose as a feedstock might be due to the difficulty in the breaking of the α -1,4-glucosidic bond of glucose and its stable pyranoside ring structure hindered the dehydration efficiency.⁶² However, fructose can easily be dehydrated into 5-HMF with excellent yield due to its structure.



View Article Online
DOI: 10.1039/D0NJ04151C

Fig. 15 Dehydration of glucose and fructose over 0.5 M $\text{SO}_4^{2-}/\text{TiO}_2$ catalyst.

Reaction condition: 1 g substrate, 0.5 g catalyst, 10 mL DMSO, at 150 °C, 6 h

3.3 Regeneration and recycle of catalyst

To determine the stability and reusability of 0.5 M $\text{SO}_4^{2-}/\text{TiO}_2$ catalyst, recycle experiments were performed at the optimized reaction condition obtained in the previous section. For the recycle experiment, two different types of catalyst reactivation strategies were performed. Results obtained were compared with the fresh catalyst which is shown in Fig. 16.

In the first strategy, the reaction mixture was centrifuged after each cycle of an experiment to recover the solid catalyst followed by washing with acetone and distilled water, respectively. The purpose of acetone washing was to remove the adsorbed organic polymer or humins adsorbed on the used catalyst surface. The washed catalyst was dried overnight at 80 °C in an oven and thereafter SO_4^{2-} group was impregnated following a similar approach. Further, the catalyst was calcined for 3 h at 550 °C in presence of air. The purpose of calcination was to remove the deposited brown organic compound on the catalyst surface and also to

1
2
3
4
5
6
7
8
9
10
11
12
13
14
15
16
17
18
19
20
21
22
23
24
25
26
27
28
29
30
31
32
33
34
35
36
37
38
39
40
41
42
43
44
45
46
47
48
49
50
51
52
53
54
55
56
57
58
59
60

reactivate the catalyst active sites. A similar regeneration strategy of the sulfate group is also reported by Suzuki et al.⁶³ The regenerated catalyst was further tested in the next cycle of the experiment and this process was repeated after each recycles experiment. The obtained catalytic performance of the regenerated 0.5 M SO₄²⁻/TiO₂ catalyst is displayed in Fig. 16. It was perceived that the activity as well as the yield of 5-HMF reduced in each cycle and after cycle-3, glucose conversion, and 5-HMF yield reduced to 67.1% and 20.7%, respectively.

In the second strategy, after washing the used catalyst by water and acetone, it was dried overnight at 80 °C followed by calcination at 400 °C for 1 h in the air.⁵⁶ After the calcination, the SO₄²⁻ group was impregnated in the catalyst following a similar approach as mentioned in the catalyst synthesis section. This regenerated catalyst was examined at optimized reaction conditions. Results (Fig. 16) demonstrated exactly similar catalytic activity and 5-HMF yield as of fresh sulfated catalyst up to several cycles.

This recycle study suggested that during the reaction, the organic polymer compounds formed, basically covered and remained adsorbed at the active surface as well as pores of the catalyst. Complete removal of these deposited organic compounds was very crucial to get back its original activity. In the first strategy, after drying the removal of these organic polymers was incomplete, as a result, the active centers for SO₄²⁻ group incorporation on the catalyst decreased drastically in the successive recycles. Only acetone washing and low-temperature drying were not enough for the complete elimination of bounded organic polymers from the catalyst pores and surface. Since the number of active centers on the catalyst surface decreased in the successive regeneration cycle, which affected the conversion of glucose and 5-HMF yield, which declined significantly after cycle-3. However, in the second strategy, SO₄²⁻ group was incorporated after the calcination of the catalyst. After calcination at the higher temperature, all the deposited organic compound was completely removed and the active centers of TiO₂ for sulfation was regenerated as a fresh one. As a result, the catalyst regenerated

following the second strategy demonstrated constant catalytic activity and 5-HMF yield after several cycles (Fig. 16). Recycle study, suggested that 0.5 M $\text{SO}_4^{2-}/\text{TiO}_2$ catalyst can be easily regenerated and reuse for several times for the effective production of 5-HMF.

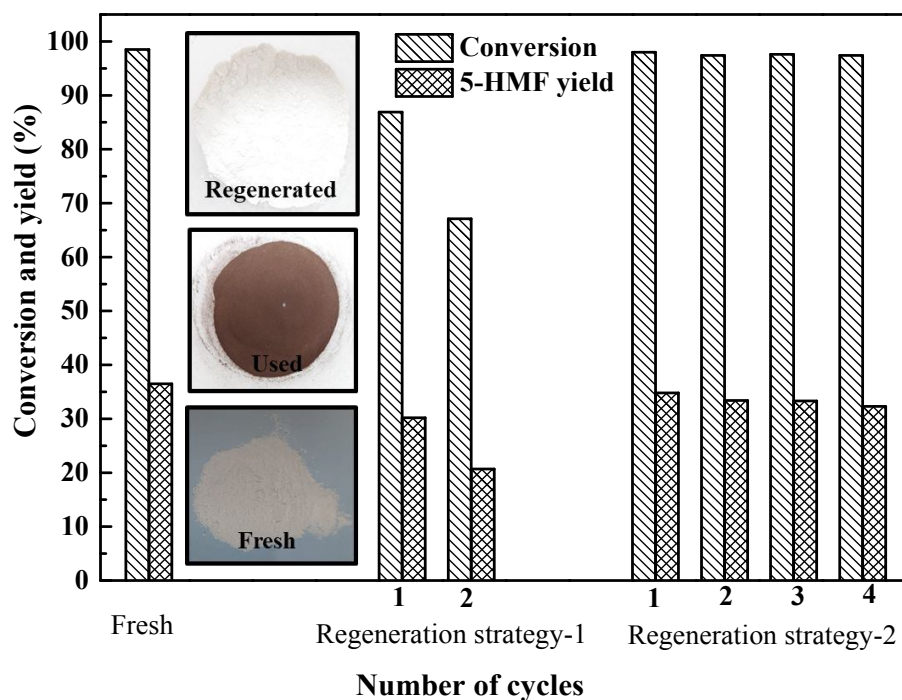


Fig. 16 Reusability experiments in presence of 0.5 M $\text{SO}_4^{2-}/\text{TiO}_2$ catalyst.

Reaction condition: 150 °C, 6 h, 10 wt.% glucose, and substrate/catalyst ratio: 2:1.

3.4 Characterizations of used catalyst

To find out the reason for the deactivation of the catalyst after cycle-1, the used catalyst was characterized by various techniques such as XRD, FTIR, and XPS (Fig. 17(A-C)). The XRD pattern (Fig. 17(A)) of the used catalyst looks similar to the pure anatase TiO_2 (Fig. 2), the XRD peaks corresponding to $\text{TiO}(\text{SO}_4)$ at the 2θ value of 16.2, 21.3, 22.2, 23.7, 27.6 and 28.2 was absent. This result depicted that, sulfate group was leached out into the reaction mixture and the sulfated catalyst returned backed to pure anatase TiO_2 after each cycle.

FTIR spectra of the used catalysts are shown in Fig. 17(B)). The intensity of the sulfate band ($900\text{-}1300\text{ cm}^{-1}$) was found to be decreased significantly. These results also supported the leaching of sulfate to some extent in the reaction medium. The H-O-H band observed for the

used catalyst was broader than the fresh one, this indicated the adsorption of a water molecule on the catalyst surface during the reaction.

In addition to these, some other stretching bands corresponding to other functional groups were also detected in the FTIR of the used catalyst (Fig. 17 (B)). The presence of humin was confirmed from the band observed at 871.33 cm^{-1} correspondings to the furan ring C-H deformation starching (out of the plane) and 1713.02 cm^{-1} bands corresponding to the C=C stretching of the furan ring, respectively.^{64,65} The band spectrum detected due the C-O and C=O stretching at the Wavenumber of $1407\text{-}1535.9\text{ cm}^{-1}$, and 1795.9 cm^{-1} , confirmed the presence of aldehyde, ketones, and acids respectively. A wideband spectrum detected at $2800\text{-}2990\text{ cm}^{-1}$ indicated the presence of methyl and methylene groups.⁶⁵

In the XPS spectra, the peak intensity of Ti, O, and S was found to be reduced significantly and peak intensity corresponding to C increased in the survey scan (Fig. 17(C)). In the case of Ti 2p, the peak of $2p_{3/2}$ was almost returned to its original position (458.5 eV and 464.6 eV) as observed for fresh TiO_2 (Fig. 6). These results confirmed the leaching of the sulfate group after the reaction. In addition to that, a combined peak is observed at 459.7 eV indicated the remaining sulfate groups were still attached in the used catalyst. The peaks corresponding to O 1s were much broader and shifted towards slightly higher binding energy (530.2 eV and 532.5 eV), which indicated the adsorption of water as well as other organic polymeric compounds during the reaction. The peak detected at 530.2 eV was due to the O-Ti-O bond of TiO_2 and the peak at 532.5 eV binding energy was due to the O-H bond of the adsorbed water molecule and C=O bond of an organic molecule adsorbed, respectively. The intensity of the XPS peaks of S 2p (S $2p_{1/2}$ and S $2p_{3/2}$) were found to be decreased significantly due to the leaching of the sulphate group in the reaction mixture. The intensity of the peaks corresponding to Ti was also decreased might be due to the catalyst surface coverage by humin or other organic polymers.

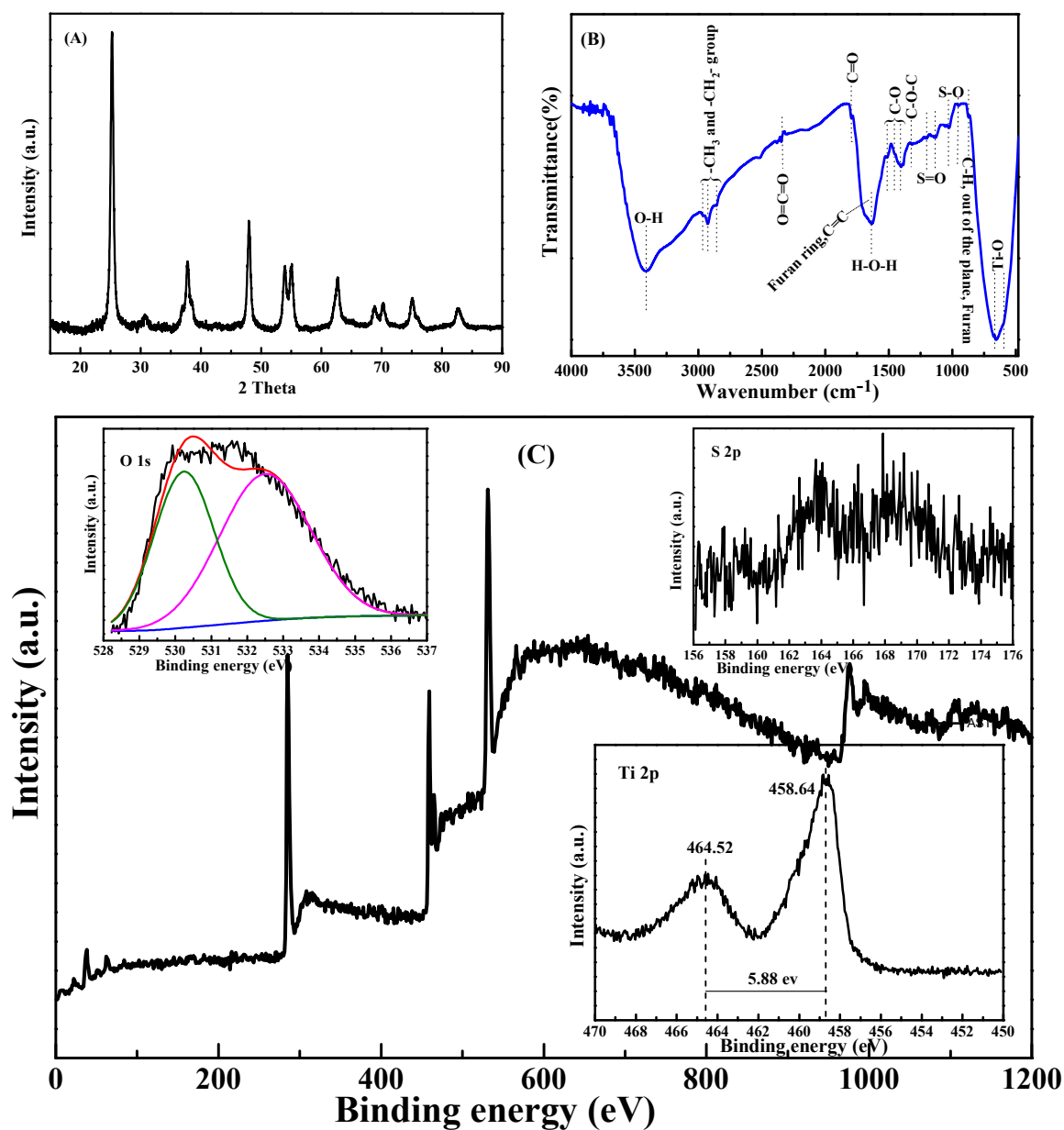


Fig. 17 Characterization of used catalyst (A) XRD pattern (B) FT-IR spectra (C) XPS spectra.

The ion chromatography analysis of the retentate obtained after the separation of catalyst from the reaction mixture also suggested the leaching of sulfate ion into the reaction mixture. The ion chromatogram of the retentate is given in the supplementary file (Fig. S3).

4. Glucose dehydration kinetics over 0.5 M SO₄²⁻/TiO₂ catalyst

The development of a realistic kinetic model and the estimation of kinetic parameters is essential to design a reactor and the overall process of an unknown reaction. The kinetic analysis essentially helps to understand better the insights of a reaction. Dehydration of glucose and fructose to 5-HMF is relatively new and the kinetics of this reaction are not well studied. Few studies focused on the basic Power-law model and fitted the glucose/fructose conversion to 5-HMF data in the first order and second-order model, respectively (Qi et al.,⁶⁶ Hu et al.,⁶⁷ and Rasrendra et al.⁶⁸). The rate constants were estimated by fitting the glucose concentrations at low conversion and Arrhenius equations were used to calculate the activation energy and pre-exponential factor for this reaction. Ramli and Amin⁶⁹ considered two more products i.e. humin, and levulinic acid in their kinetic study, and based-on a series-parallel reaction scheme, the kinetic model was developed following the Power-law type approach. Although, the Power-law model does not incorporate realistic heterogeneous kinetic phenomena such as adsorption, surface reaction, and desorption. However, the kinetic data obtained from the Power-law model may be used as an initial guess for the determination of the kinetic parameters of a realistic heterogeneous kinetic model.

In this study, the preliminary kinetic analysis and the estimation of kinetic parameters were performed following the Power-law approach. Experimental results suggested that the reaction temperature and time was the most influencing reaction parameter for glucose conversion and 5-HMF yield. Therefore, to determine the activation energy and pre-exponential factor, the kinetic experiments were carried out at various temperatures (130-160 °C) in presence of a 0.5 M $\text{SO}_4^{2-}/\text{TiO}_2$ catalyst. Other reaction parameters such as catalyst amount, glucose concentration, the solvent volume may affect the kinetics were kept constant. Products were collected at a regular time interval and the concentration of glucose was monitored. It was found that glucose conversion was varied rapidly at the initial hour of the reaction (Fig. 11), therefore, the kinetic data were collected at the initial hour (< 1 h) of the

reaction. To determine the kinetic parameter, initially, first-order glucose dehydration reaction was considered. By following Levenspiel approach,^{67,68} the rate of disappearance of glucose was expressed as:

$$\frac{dC_A}{dt} = -kC_A \quad (3)$$

After integration, equation (1) reduced to

$$\ln\left(\frac{C_A}{C_{A_0}}\right) = kt \quad (4)$$

where C_{A_0} and C_A were the concentration of glucose in mol. L⁻¹ at $t = 0$ and $t = t$ (min.), respectively. The obtained variation of $\ln(C_A/C_{A_0})$ as a function of time is presented in Fig. 18(A). At a particular temperature, the slope of each straight line fit represented the rate constant (k). The calculated rate constant value and linearity coefficient for each temperature is summarized in Table 2. Further, the activation energy (E) and pre-exponential factor (A_0) was calculated from the Arrhenius equation ($k = A_0 e^{E/RT}$). Due to the strong correlation between the pre-exponential factor and activation energy, re-parameterization of the Arrhenius equation was performed as follows:⁷⁰

$$k^* = A^* \exp\left[-\frac{E}{R}\left(\frac{1}{T} - \frac{1}{T^*}\right)\right] \quad (5)$$

where T^* is the average temperature and $A^* = A_0 \exp(-E/RT^*)$

Further, the equation (5) was linearized as follows:

$$\ln(k^*) = \ln(A^*) - \frac{E}{R}\left(\frac{1}{T} - \frac{1}{T^*}\right) \quad (6)$$

The activation energy (E) and the pre-exponential factor (A^*) were calculated from the slope and intercept of the plot of $\ln(k^*)$ versus $(1/T - 1/T^*)$. The calculated values of the activation energy and the frequency factor were found to be (120.8 ± 0.41) kJ. mol⁻¹ and $(2.66 \pm 0.30) \times 10^{13}$ min⁻¹, respectively and the R^2 value of the first-order fit was ~ 0.92 . These obtained activation energy and frequency factor were comparable with the value reported earlier.⁶⁶ Qi

et al.⁶⁶ reported the activation energy and frequency factor of 114.6 kJ mol⁻¹ and 3.5×10^{14} min⁻¹, respectively, for the dehydration of glucose to 5-HMF in [BMIM]Cl ionic liquid medium under microwave heating.

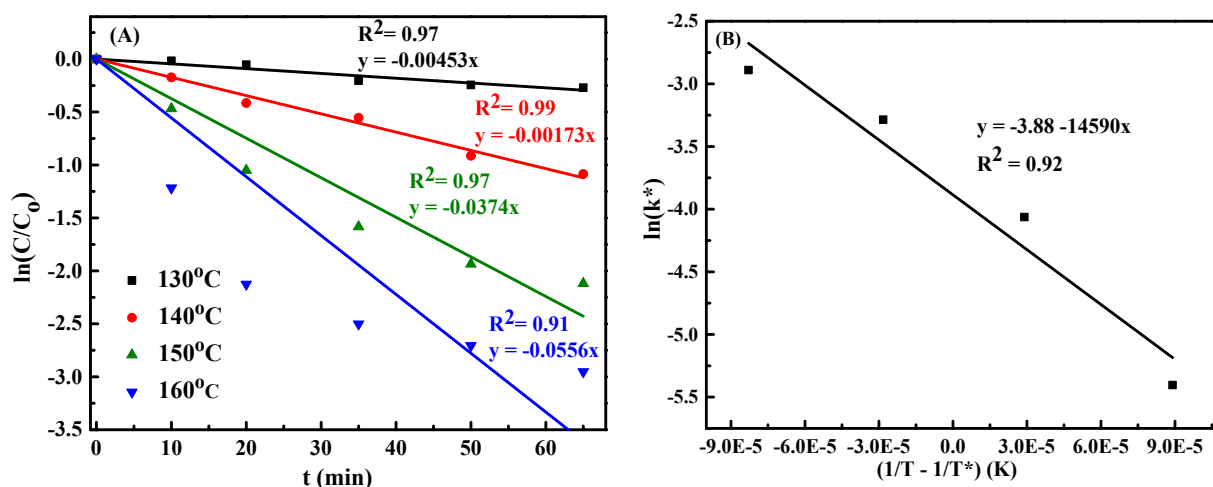
Furthermore, to improve the value of the linearity coefficient (R^2), the disappearance of glucose was assumed to be second-order dependency as reported by Rane et al.⁷¹ for esterification of glycerol. In the second-order model, the disappearance of glucose was expressed as:

$$\frac{dC_A}{dt} = kC_A^2 \quad (5)$$

On integration, equation (3) reduced to

$$\left(\frac{1}{C_A} - \frac{1}{C_{A_0}}\right) = kt \quad (6)$$

The plot of $(1/C_A)$ as a function of time (t) is shown in Fig. 18(C). The slope of each straight line in Fig. 18(C) was the rate constant (k) at that respective temperature. The calculated rate



constants and the linearity coefficients (R^2) are shown in Table 2. The rate constant was found to be increased with temperature indicated that the glucose dehydration reaction was accelerated at a higher temperature. The Arrhenius equation was re-parameterized as before and the activation energy (E) and the pre-exponential factor (A_0) were calculated. The calculated activation energy and pre-exponential factor were (195.4 ± 0.00) kJ. mol⁻¹ and $(2.27 \pm 0.00) \times 10^{20}$ L mol⁻¹ s⁻¹, respectively. The R^2 value obtained for second-order fit was close to 1, which suggested that glucose dehydration reaction over 0.5 M SO₄²⁻/TiO₂ catalysts in the DMSO medium followed the second-order dependency. For the second-order glucose dehydration reaction with metal salt (Al(OTf₃)) in the DMSO medium under microwave heating, Rasrendra et al.⁶⁸ found the value of activation energy and frequency factor of 138 kJ mol⁻¹ and 4.7×10^{17} min⁻¹, respectively. The difference in activation energy and frequency factor might be due to the divergence in reaction circumstances such as catalyst, solvent, and heating medium, etc.

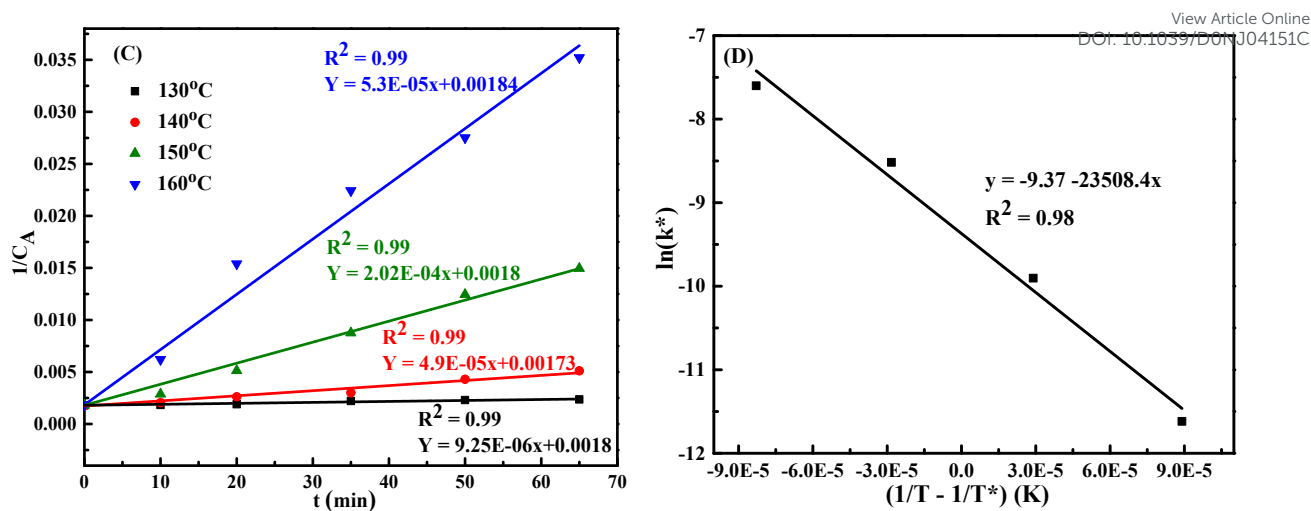


Fig. 18 Kinetics curves of glucose dehydration reaction (A) First order fit (B) Arrhenius plot for first order (C) second-order fit (D) Arrhenius plot for second-order.

Table 2 Kinetic parameters for glucose dehydration to 5-HMF

Temperature (°C)	First-order dependence		Second-order dependence	
	Rate constant (s ⁻¹)	R ²	Rate constant (L mol ⁻¹ s ⁻¹)	R ²
130	0.0045	0.97	9.25×10^{-6}	0.99
140	0.0172	0.99	4.90×10^{-5}	0.99
150	0.0374	0.97	2.02×10^{-4}	0.99
160	0.0556	0.91	5.31×10^{-4}	0.99
Activation Energy	(120.8 ± 0.41) kJ. mol ⁻¹		(195.4 ± 0.00) kJ. mol ⁻¹	
Frequency factor	$(2.66 \pm 0.30) \times 10^{13}$ min ⁻¹		$(2.27 \pm 0.00) \times 10^{20}$ L mol ⁻¹ s ⁻¹	

Conclusions

Various sulfated Titania (SO₄²⁻/TiO₂) catalyst was prepared by sol-gel hydrolysis and wetness impregnation method for the dehydration of glucose and fructose to 5-HMF. Catalyst characterization results demonstrated the typical mesoporous nature of catalysts. The surface area and pore size of catalysts were found to be decreased by increasing the concentration of sulfate ion in anatase TiO₂ because of pore blockage. The total acidic strength of the catalyst was found to be enhanced after the impregnation of the sulfate group and it was highest (0.57

mmol g⁻¹) for 0.5 M SO₄²⁻/TiO₂ among all other catalysts. The ratio of Lewis and Brønsted acidic strength of the catalyst was tuned by altering the sulfate concentration and measured by using pyridine FTIR. The sulfonic group was the main source of Brønsted acidity of the catalyst. XPS results dictated the oxidation state of Ti was in +4 state in the catalyst, and it was unchanged after sulfation.

For glucose dehydration reaction the major reaction products were 5-HMF, LA, FA, and black organic polymer might be humin. The reaction followed isomerization-hydration-rehydration mechanism over the SO₄²⁻/TiO₂ catalyst. The yield of the products was highly dependent on temperature. Higher temperature (> 150 °C), time (> 6 h), catalyst amount (> 0.5 g) was not useful for higher 5-HMF yield, which favored the degradation of glucose and 5-HMF to other soluble and insoluble dark-colored organic polymers. It was observed that in an organic medium, the yield of 5-HMF was higher due to hindrance in rehydration of 5-HMF. Among all catalyst tested, 0.5 M SO₄²⁻/TiO₂ catalyst was found to be more effective. In presence of glucose as a feedstock, a maximum 5-HMF yield of ~37% was achieved with 98.3% conversion of glucose at 150 °C after 6 h. However, the 5-HMF yield was significantly higher (74.7%) in presence of fructose as a feedstock. The lower yield of 5-HMF with glucose was due to the difficulty in breaking of the α -1,4-glucosidic bond of glucose and its stable pyranoside ring structure. An appropriate balance of Lewis and Brønsted acidic sites in the catalyst played an important role in glucose isomerization followed by fructose dehydration to 5-HMF. A new catalyst regeneration study was developed and it was established that 0.5 M SO₄²⁻/TiO₂ catalyst can be regenerated and reuse several times with constant activity and 5-HMF yield. Finally, the kinetic experiments were carried out to determine the kinetic variables for glucose dehydration reaction. The power-law model was used to determine the activation energy and pre-exponential factor, and glucose conversion data was better fitted with the

second-order kinetics. Based on the power-law model, the calculated activation energy and pre-exponential factor were 195.4 kJ mol⁻¹ and of 2.27×10^{20} L mol⁻¹ s⁻¹, respectively.

Conflicts of interests

There are no conflicts to declare.

Acknowledgment

The author kindly acknowledges the Ministry of Human Resource and Development, Government of India for financial support, and Indian Institute of Technology Roorkee for providing necessary facilities to carry out the work.

Funding

This work is supported by the Indian Institute of Technology Roorkee, Roorkee, Uttarakhand, India. Student fellowship is supported by the Ministry of Human Resource Development (MHRD), Government of India.

References

- 1 J. Guo, S. Zhu, Y. Cen, Z. Qin, J. Wang and W. Fan, *Appl Catal B Environ*, 2017, **200**, 611–619.
- 2 A. Corma Canos, S. Iborra and A. Velyt, *Chem Rev*, 2007, 107, 2411–2502.
- 3 T. Wang, J. A. Glasper and B. H. Shanks, *Appl Catal A Gen*, 2015, **498**, 214–221.
- 4 M. Zhang, K. Su, H. Song, Z. Li and B. Cheng, *Catal Commun*, 2015, **69**, 76–80.
- 5 M. K. Shukla, E. Singh, N. Singh and S. K. Singal, *J Mater Cycles Waste Manag*, 2015, **17**, 459–464.
- 6 G. Portillo Perez and M. J. Dumont, *Chem Eng J*, 2020, **382**, 122766.
- 7 M. Nahavandi, T. Kasanneni, Z. S. Yuan, C. C. Xu and S. Rohani, *ACS Sustain Chem Eng*, 2019, **7**, 11970–11984.

- 1
2
3
4
5
6
7
8
9
10
11
12
13
14
15
16
17
18
19
20
21
22
23
24
25
26
27
28
29
30
31
32
33
34
35
36
37
38
39
40
41
42
43
44
45
46
47
48
49
50
51
52
53
54
55
56
57
58
59
60
- 8 V. Choudhary, S. H. Mushrif, C. Ho, A. Anderko, V. Nikolakis, N. S. Marinkovic, A. I. Frenkel, S. I. Sandler and D. G. Vlachos, *J Am Chem Soc*, 2013, **135**, 3997–4006. View Article Online
DOI: 10.1039/C3DNJ04151C
- 9 T. Ji, Z. Li, C. Liu, X. Lu, L. Li and J. Zhu, *Appl Catal B Environ*, 2019, **243**, 741–749.
- 10 Y. He, A. K. Itta, A. A. Alwakwak, M. Huang, F. Rezaei and A. A. Rownaghi, *ACS Sustain Chem Eng*, 2018, **6**, 17211–17219.
- 11 F. Shahangi, A. Najafi Chermahini and M. Saraji, *J Energy Chem*, 2018, **27**, 769–780.
- 12 P. Ganji and S. Roy, *Energy and Fuels*, 2019, **33**, 5293–5303.
- 13 K. Nakajima, R. Noma, M. Kitano and M. Hara, *J Mol Catal A Chem*, 2014, **388–389**, 100–105.
- 14 M. Watanabe, Y. Aizawa, T. Iida, T. M. Aida, C. Levy, K. Sue and H. Inomata, *Carbohydr Res*, 2005, **340**, 1925–1930.
- 15 S. P. Utami and N. S. Amin, *Ind Crops Prod*, 2013, **41**, 64–70.
- 16 S. Jia, Z. Xu and Z. C. Zhang, *Chem Eng J*, 2014, **254**, 333–339.
- 17 Y. M. Lu, H. Li, J. He, Y. X. Liu, Z. B. Wu, D. Y. Hu and S. Yang, *RSC Adv*, 2016, **6**, 12782–12787.
- 18 H. Yan, Y. Yang, D. Tong, X. Xiang and C. Hu, *Catal Commun*, 2009, **10**, 1558–1563.
- 19 K. V. Wagh, K. C. Badgujar, N. M. Patil and B. M. Bhanage, *Curr Org Chem*, 2016, **20**, 736–751.
- 20 D. Chen, F. Liang, D. Feng, M. Xian, H. Zhang, H. Liu and F. Du, *Chem Eng J*, 2016, **300**, 177–184.

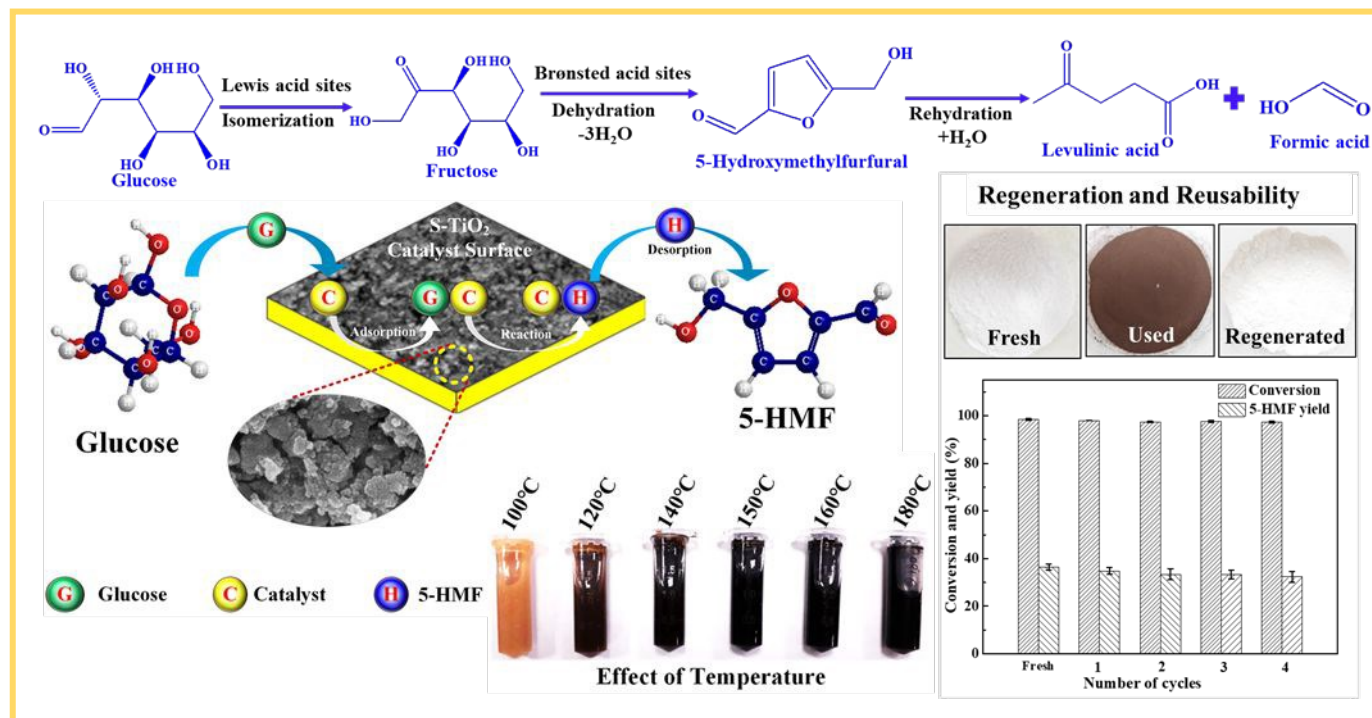
- 1
2
3
4
5
6
7
8
9
10
11
12
13
14
15
16
17
18
19
20
21
22
23
24
25
26
27
28
29
30
31
32
33
34
35
36
37
38
39
40
41
42
43
44
45
46
47
48
49
50
51
52
53
54
55
56
57
58
59
60
- 21 A. Mukherjee, M. J. Dumont and V. Raghavan, *Biomass and Bioenergy*, 2015, **72**, 143–183. View Article Online
DOI:10.1039/D0NJ04151C
- 22 S. P. Teong, G. Yi and Y. Zhang, *Green Chem*, 2014, **16**, 2015.
- 23 X. Wang, T. Lv, M. Wu, J. Sui, Q. Liu, H. Liu, J. Huang and L. Jia, *Appl Catal A Gen*, 2019, **574**, 87–96.
- 24 R. Otomo, T. Yokoi, J. N. Kondo and T. Tatsumi, *Appl Catal A Gen*, 2014, **470**, 318–326.
- 25 I. Jiménez-Morales, M. Moreno-Recio, J. Santamaría-González, P. Maireles-Torres and A. Jiménez-López, *Appl Catal B Environ*, 2015, **164**, 70–76.
- 26 C. Fan, H. Guan, H. Zhang, J. Wang, S. Wang and X. Wang, *Biomass and Bioenergy*, 2011, **35**, 2659–2665.
- 27 C. García-Sancho, I. Fúnez-Núñez, R. Moreno-Tost, J. Santamaría-González, E. Pérez-Inestrosa, J. L. G. Fierro and P. Maireles-Torres, *Appl Catal B Environ*, 2017, **206**, 617–625.
- 28 Y. Feng, M. Zuo, T. Wang, W. Jia, X. Zhao, X. Zeng, Y. Sun, X. Tang, T. Lei and L. Lin, *J Taiwan Inst Chem Eng*, 2019, **96**, 431–438.
- 29 M. Ohara, A. Takagaki, S. Nishimura and K. Ebitani, *Appl Catal A Gen*, 2010, **383**, 149–155.
- 30 Y. Qu, C. Huang, Y. Song, J. Zhang and B. Chen, *Bioresour Technol*, 2012, **121**, 462–466.
- 31 J. Liu, H. Li, Y. C. Liu, Y. M. Lu, J. He, X. F. Liu, Z. B. Wu and S. Yang, *Catal Commun*, 2015, **62**, 19–23.

- 1
2
3
4
5
6
7
8
9
10
11
12
13
14
15
16
17
18
19
20
21
22
23
24
25
26
27
28
29
30
31
32 J. B. Binder and R. T. Raines, *J Am Chem Soc*, 2009, **131**, 1979–1985. View Article Online
DOI: 10.1039/D0NJ04151C
- 33 L. Körösi, S. Papp, I. Bertóti and I. Dékány, *Chem Mater*, 2007, **19**, 4811–4819.
- 34 M. Hosseini-Sarvari, E. Sodagar and M. M. Doroodmand, *J Org Chem*, 2011, **76**,
2853–2859.
- 35 N. A. S. Ramli and N. A. S. Amin, *Appl Catal B Environ*, 2015, **163**, 487–498.
- 36 K. J. A. Raj and B. Viswanathan, *ACS Appl Mater Interfaces*, 2009, **1**, 2462–2469.
- 37 S. M. Patil, S. P. Deshmukh, K. V. More, V. B. Shevale, S. B. Mullani, A. G.
Dhodamani and S. D. Delekar, *Mater Chem Phys*, 2019, **225**, 247–255.
- 38 A. V. Nakhate, S. M. Doke and G. D. Yadav, *Ind Eng Chem Res*, 2016, **55**, 10829–
10838.
- 39 J. Gardy, A. Hassanpour, X. Lai and M. H. Ahmed, *Appl Catal A Gen*, 2016, **527**, 81–
95.
- 40 M. K. Lam, K. T. Lee and A. R. Mohamed, *Appl Catal B Environ*, 2009, **93**, 134–139.
- 41 Z. Huang, Y. Lin, L. Li, C. Ye and T. Qiu, *Chinese J Chem Eng*, 2017, **25**, 1207–1216.
- 42 Y. Niu, F. Li, K. Yang, T. Qiu, R. Wang and C. Lin, *Chinese J Chem Eng*, 2016, **24**,
767–774.
- 43 Y. Yuan, W. Jiang and J. Li, *Chinese J Chem Eng*, 2019, **27**, 2696–2704.
- 44 A. K. Dalai, R. Sethuraman, S. P. R. Katikaneni and R. O. Idem, *Ind Eng Chem Res*,
1998, **37**, 3869–3878.
- 45 L. K. Noda, R. M. De Almeida, N. S. Gonçalves, L. F. D. Probst and O. Sala, *Catal
Today*, 2003, **85**, 69–74.

- 1
2
3
4
5
6
7
8
9
10
11
12
13
14
15
16
17
18
19
20
21
22
23
24
25
26
27
28
29
30
31
32
33
34
35
36
37
38
39
40
41
42
43
44
45
46
47
48
49
50
51
52
53
54
55
56
57
58
59
60
- 46 A. A. Dabbawala, S. M. Alhassan, D. K. Mishra, J. Jegal and J. S. Hwang, *Mol Catal*, 2018, **454**, 77–86. View Article Online
DOI: 10.1039/C8NJ04151C
- 47 L. Li, H. Yue, T. Ji, W. Li, X. Zhao, L. Wang, J. She, X. Gu and X. Li, *Appl Catal A Gen*, 2019, **574**, 25–32.
- 48 X. Bai, L. Pan, P. Zhao, D. Fan and W. Li, *Cuihua Xuebao/Chinese J Catal*, 2016, **37**, 1469–1476.
- 49 G. Colón, M. C. Hidalgo, J. A. Navío, A. Kubacka and M. Fernández-García, *Appl Catal B Environ*, 2009, **90**, 633–641.
- 50 M. Hamadani, A. Reisi-Vanani and A. Majedi, *Mater Chem Phys*, 2009, **116**, 376–382.
- 51 K. Nagaveni, M. S. Hegde and G. Madras, *J Phys Chem B*, 2004, **108**, 20204–20212.
- 52 D. K. Pandey and P. Biswas, *New J Chem*, 2019, **43**, 10073–10086.
- 53 K. R. Sunajadevi and S. Sugunan, *Mater Lett*, 2006, **60**, 3813–3817.
- 54 T. Bezrodna, G. Puchkovska, V. Shimanovska, I. Chashechnikova, T. Khalyavka and J. Baran, *Appl Surf Sci*, 2003, **214**, 222–231.
- 55 H. Li, M. Vrinat, G. Berhault, D. Li, H. Nie and P. Afanasiev, *Mater Res Bull*, 2013, **48**, 3374–3382.
- 56 H. Zhao, P. Jiang, Y. Dong, M. Huang and B. Liu, *New J Chem*, 2014, **38**, 4541–4548.
- 57 S. Yamazaki, N. Fujinaga and K. Araki, *Appl Catal A Gen*, 2001, **210**, 97–102.
- 58 G. Durango-Giraldo, A. Cardona, J. F. Zapata, J. F. Santa and R. Buitrago-Sierra, *Heliyon*, 2019, **5**, e01608.
- 59 J. R. Sohn, S. H. Lee, P. W. Cheon and H. W. Kim, *Bull Korean Chem Soc*, 2004, **25**,

- 657–664.
- 60 H. Esteban Benito, T. Del Ángel Sánchez, R. García Alamilla, J. M. Hernández Enríquez, G. Sandoval Robles and F. Paraguay Delgado, *Brazilian J Chem Eng*, 2014, **31**, 737–745.
- 61 A. Teimouri, M. Mazaheri, A. N. Chermahini, H. Salavati, F. Momenbeik and M. Fazel-Najafabadi, *J Taiwan Inst Chem Eng*, 2015, **49**, 40–50.
- 62 L. Zhang, G. Xi, Z. Chen, Z. Qi and X. Wang, *Chem Eng J*, 2017, **307**, 877–883.
- 63 T. Suzuki, T. Yokoi, R. Otomo, J. N. Kondo and T. Tatsumi, *Appl Catal A Gen*, 2011, **408**, 117–124.
- 64 C. B. Rasrendra, M. Windt, Y. Wang, S. Adisasmito, I. G. B. N. Makertihartha, E. R. H. Van Eck, D. Meier and H. J. Heeres, *J Anal Appl Pyrolysis*, 2013, **104**, 299–307.
- 65 S. Wang, H. Lin, J. Chen, Y. Zhao, B. Ru, K. Qiu and J. Zhou, *RSC Adv*, 2015, **5**, 84014–84021.
- 66 X. Qi, M. Watanabe, T. M. Aida and R. L. Smith, *ChemSusChem*, 2010, **3**, 1071–1077.
- 67 L. Hu, Z. Wu, J. Xu, Y. Sun, L. Lin and S. Liu, *Chem Eng J*, 2014, **244**, 137–144.
- 68 C. B. Rasrendra, J. N. M. Soetedjo, I. G. B. N. Makertihartha, S. Adisasmito and H. J. Heeres, *Top Catal*, 2012, **55**, 543–549.
- 69 N. A. S. Ramli and N. A. S. Amin, *Chem Eng J*, 2016, **283**, 150–159.
- 70 N. Brauner and M. Shacham, *Chem Eng Process Process Intensif*, 1997, **36**, 243–249.
- 71 S. A. Rane, S. M. Pudi and P. Biswas, *Chem Biochem Eng Q*, 2016, **30**, 33–45.

Graphical abstract

View Article Online
DOI: 10.1039/D0NJ04151C

Research highlights

- A very efficient SO₄²⁻/TiO₂ solid acid catalyst was developed by sol-gel hydrolysis followed by the wetness impregnation method, for the dehydration of glucose/fructose to 5-hydroxymethylfurfural (5-HMF).
- A maximum of ~75% and ~37% yield of 5-HMF was achieved in presence of fructose and glucose as a feed-in the DMSO solvent, respectively.
- Tunable Lewis and Brønsted acidic strength of the catalyst played a crucial role in the higher yield of 5-HMF.
- SO₄²⁻/TiO₂ catalyst can be efficiently regenerated and recycled several times with constant activity and 5-HMF yield.
- A power-law model was developed for the conversion of glucose to 5-HMF and the experimental data was best fitted to second-order kinetics.